

1 Expansion of apical extracellular matrix underlies the 2 morphogenesis of a recently evolved structure

3
4 Sarah Jacquelyn Smith¹, Lance A. Davidson², Mark Rebeiz^{1*}

5
6 ¹ University of Pittsburgh Department of Biological Sciences, Pittsburgh, PA 15260, United States.

7 ² University of Pittsburgh, Department of Bioengineering, Pittsburgh, PA 15260, United States.

8
9 *Corresponding author: rebeiz@pitt.edu

10

11

12 **Abstract**

13 One of the fundamental gaps in our knowledge of the evolution of novel structures is
14 understanding how the morphogenetic processes that form these structures arise. Here, we
15 traced the cellular development of a morphological novelty, the posterior lobe of *D.*
16 *melanogaster*. We found that this genital outgrowth forms through an extreme increase in cell
17 height. By examining the apical extracellular matrix (aECM), we uncovered a vast network
18 associated with the developing genitalia of lobed and non-lobed species. We observed that cells
19 which will form the posterior lobe show expanded expression of the aECM protein Dumpy which
20 connects them to the ancestral aECM network. Further analysis demonstrated a required role
21 for Dumpy in cell height increase during development. We propose that the aECM presents a
22 rich reservoir for generating morphological novelty, in addition to highlighting a yet unseen role
23 for aECM in regulating extreme cell height.

24 **Introduction**

25 Biologists have long been mesmerized by the appearance of morphological novelties, new
26 structures that appear to lack homologs in other species groups (Moczek, 2008; Günter et al.,
27 2010). To understand the origins of these novel structures, significant effort has focused on
28 determining how spatial and temporal patterning of genes are altered during evolution (Peter &
29 Davidson, 2015; Rebeiz, et al., 2015; Wagner, 2014). This has indicated how developmental
30 programs are often associated with morphological novelties, and they are frequently co-opted
31 from other tissues. However, limited attention has been directed to how novel structures form at
32 the cellular level. Understanding how a structure physically forms is important, as it can help
33 explain which morphogenetic processes might be targeted during evolution. In addition,
34 because most morphological novelties arose in the distant past, it is likely that the causative

35 genetic changes will be obscured by additional changes scattered throughout relevant gene
36 regulatory networks (Liu, Y., 2019). Hence, understanding the morphogenetic basis of a novelty
37 is critical to identifying the most important aspects of the gene regulatory networks that
38 contributed to its origin.

39

40 Most studies of morphogenetic evolution have focused on structures subject to diversification,
41 illuminating processes that contributed to their modification, as opposed to origination. For
42 example, studies of tooth morphogenesis have elucidated how both internal mechanisms, such
43 as cell shape changes (Li et al., 2016), and external forces, such as the pressure from the
44 surrounding jaw (Renvoisé et al., 2017) could be contributing factors in their diversification. A
45 study of the enlarged ovipositor of *Drosophila suzukii* revealed how a 60% increase in length
46 was associated with increases in apical area and anisotropic cellular rearrangement (Green et
47 al., 2019). In addition, differences in early morphogenetic mechanisms between distantly related
48 species are observed in both the development of breathing tubes on the Drosophilid eggshell
49 (Osterfield et al., 2015) and migration of sex comb precursors on *Drosophila* male forelegs
50 (Atallah et al., 2009; Tanaka et al., 2009), together highlighting how rapid changes in
51 morphogenetic mechanisms can evolve to form the same structure. Overall, these studies have
52 illustrated how evolutionary comparative approaches can reveal morphogenetic processes
53 critical to the sculpting of anatomical structures.

54

55 Morphogenesis is the product of both cell intrinsic processes, such as those conferred by the
56 cytoskeleton or cell-cell junctions, and external forces from the environment in which the cell
57 resides. Extracellular mechanics are relatively understudied compared to intracellular
58 mechanics (Paluch & Heisenberg, 2009). An important component of the microenvironment of a
59 cell is the extracellular matrix (ECM) which can be subdivided into two populations of ECM, the
60 basal ECM and the apical ECM (aECM) (Brown, 2011; Daley & Yamada, 2013; Linde-Medina &
61 Marcucio, 2018; Loganathan et al., 2016). While comparatively understudied, recent work has
62 defined vital roles for aECM in the morphogenesis of the *Drosophila* wing (Diaz-de-la-Loza et
63 al., 2018; Etournay et al., 2015; Ray et al., 2015), denticles (Fernandes et al., 2010), and
64 trachea (Dong et al., 2014) , as well as the *C. elegans* excretory system (Mancuso et al., 2012).
65 Despite recent interest in the aECM, its role in the evolution of morphogenetic processes is
66 currently unknown.

67

68 Genital traits represent a particularly advantageous system in which to study the morphogenetic
69 basis of novel structures. The study of morphological novelty is often difficult because most
70 structures of interest evolved in the distant past, rendering it difficult to understand the ancestral
71 ground state from which the novelty emerged. Genitalia are noted for their rapid evolution
72 (Eberhard, 1985), and thus bear traits among closely-related species that have recently evolved
73 in the context of a tissue that is otherwise minimally altered. For example, the posterior lobe, a
74 recently evolved anatomical structure present on the genitalia of male flies of the *melanogaster*
75 clade (Kopp & True, 2002) (Figure 1A), is a three-dimensional outgrowth that is required for
76 genital coupling (Frazee & Masly, 2015; Jagadeeshan & Singh, 2006; LeVasseur-Viens et al.,
77 2015). Besides the posterior lobe, the genitalia of lobed and non-lobed species are quite similar
78 in composition, providing an excellent context in which to examine the morphogenesis of the
79 ancestral structures from which the posterior lobe emerged.

80

81 Here, we find cell shape changes which increase cell height along the apico-basal axis drive
82 morphogenesis of the posterior lobe. We investigated internal and external factors that might
83 contribute to this height increase and find a correlation between the aECM protein Dumpy and
84 the height of posterior lobe cells. Comparisons to non-lobed species uncovered the presence of
85 a conserved aECM network on the genitalia that has expanded to cells that form the posterior
86 lobe. Our work shows how the formation of a morphological novelty depends upon novel aECM
87 attachments, integrating cells into a larger pre-existing aECM network.

88 **Results**

89 **The posterior lobe grows from the lateral plate epithelium**

90 The male genitalia of *Drosophila* is a bilaterally symmetrical anatomical structure which forms
91 from the genital disc during pupal development. In adults, the posterior lobe protrudes from a
92 structure called the lateral plate (also known as the ventral epandrial ventral lobe (Rice et al.,
93 2019)) (Figure 1A,D; Figure 1 - video 1). In *D. melanogaster*, prior to posterior lobe formation,
94 the lateral plate is fully fused to a neighboring structure called the clasper (also known as the
95 surstylus (Rice et al., 2019)) (Figure 1B) (Glassford et al., 2015). The lateral plate begins to
96 separate from the clasper around 32 hours after pupal formation (APF) in *D. melanogaster*.
97 Approximately 4 hours later, the posterior lobe begins to project from the plane of the lateral
98 plate and achieves its final shape by 52 hours APF (Figure 1D; Figure 1- supplement 1). During
99 posterior lobe development, cleavage of the lateral plate from the clasper continues, dropping

100 the tip of the lateral plate behind the clasper and separating both tissues (Figure 1D; Figure 1 -
101 supplement 1). Full separation of the lateral plate and clasper stops slightly above (ventral to)
102 the posterior lobe (Figure 1 - supplement 1). By contrast, the lateral plate in the non-lobed
103 species *D. biarmipes*, remains flat throughout development, but all other morphogenetic events
104 are very similar, forming on a schedule that is approximately 4 hours behind *D. melanogaster*
105 (Figure 1C,E; Figure 1 - supplement 1).

106

107 **Posterior lobe cells increase in height to protrude from the lateral plate**

108 To investigate which cellular behaviors are unique to lobed species, we examined how the
109 posterior lobe grows from the lateral plate in both lobed and non-lobed species. First, we looked
110 at cell proliferation, which commonly contributes to morphogenesis through patterned and/or
111 oriented cell division (Heisenberg & Bellaïche, 2013), such as observed during branching
112 morphogenesis in the lung where oriented cell division expands the bud before it bifurcates into
113 two branches (Schnatwinkel & Niswander, 2013). During stages prior to the development of the
114 posterior lobe morphogenesis, we observed widespread cell proliferation throughout the entire
115 genital epithelium (Figure 2 - supplement 1). However, proliferation declines tissue-wide and all
116 cell proliferation is essentially absent during posterior lobe development (Figure 2 - supplement
117 1). Similar dynamics in proliferation are also observed in non-lobed species (Figure 2 -
118 supplement 1), suggesting that proliferation is not a major contributor to the morphogenesis of
119 the posterior lobe.

120

121 Next we tested the possibility that cell intercalation could contribute to posterior lobe
122 morphogenesis. Such processes may play a role in tissue elongation (Guirao & Bellaïche, 2017;
123 Tada & Heisenberg, 2012; Walck-Shannon & Hardin, 2014), such as in germ-band extension in
124 *Drosophila* where directed cell intercalation results in a reduction in the number of cells on the
125 anterior-posterior axis and an increase in the number of cells along the dorsal-ventral axis,
126 elongating the tissue along the dorsal-ventral axis (Irvine & Wieschaus, 1994). To test this, we
127 utilized live cell tracking during posterior lobe development. Initial observations of the outer face
128 of the posterior lobe revealed few cell rearrangement events. When cell rearrangements did
129 occur it was in response to a cell being removed from the apical surface (Figure 2 - video 1).
130 Due to the limited number of cell rearrangement events observed during posterior lobe
131 morphogenesis, cell intercalation does not appear to be a major driver of posterior lobe
132 morphogenesis, causing us to instead examine changes in cell shape.

133
134 Changes to cell shape are quite common during tissue morphogenesis, as classically illustrated
135 by the process of apical constriction that deforms tissues during many developmental processes
136 (Lecuit & Lenne, 2007; Martin & Goldstein, 2014). To examine cell shape, we utilized the
137 Raeppli system to label individual cells with a fluorescent marker (mTFP1) (Kanca et al., 2014).
138 We observed that cells within the posterior lobe are tall and thin, spanning from the basal to the
139 apical surface of the epithelium (Figure 2A). Because cells span the full thickness of this tissue,
140 we can approximate the height of the tallest cells in the posterior lobe by measuring tissue
141 thickness. For these measurements, we used the lateral plate as an in-sample comparison,
142 since it represents the tissue from which the posterior lobe protrudes and should differ from the
143 lobe in morphogenetic processes. We observed a pronounced increase in thickness of the
144 posterior lobe compared to the lateral plate (Figure 2B-C,F; Figure 2 - supplement 2). The
145 posterior lobe more than doubles in thickness with an average increase of 145.3% (+ 47.5 μ m),
146 while the lateral plate only increases by 22.6% (+ 7.9 μ m) overall. In contrast, when non-lobed
147 species are examined, no thickness changes are observed in the location where a posterior
148 lobe would form, indicating that this increase in tissue thickness is unique to the posterior lobe
149 (Figure 2B-E,G; Figure 2 - supplement 2). Interestingly, this increase in thickness is a dynamic
150 process during development. During the first 12 hours of posterior lobe development the lateral
151 plate thickness decreases by 5.1 μ m, but the posterior lobe increases in thickness by 16.5 μ m on
152 average (Figure 2F). By contrast, during the last 4 hours of development, rapid increases in
153 thickness occur in both the posterior lobe and lateral plate, which increase on average by
154 31.0 μ m and 14.6 μ m respectively (Figure 2F). These observations reveal a slow phase of cell
155 height increase during the first 12 hours of posterior lobe development, and fast phase during
156 the last four hours of posterior lobe development. Together this data suggests that the cells of
157 the posterior lobe undergo an extreme cell shape change to increase in length along their apico-
158 basal axis, driving the posterior lobe cells to project out of the plane of the lateral plate.

159 **Cytoskeletal components increase in concentration in posterior lobe cells**

160 Elongation of cells along their apico-basal axis appears to be a major contributor to posterior
161 lobe formation. To understand potential internal forces contributing to this cell shape change we
162 examined the cytoskeleton to determine if alterations in cytoskeletal organization or dynamics
163 are occurring. As expected for a well polarized epithelium, we found F-actin strongly localized to
164 the apical cortex overlapping with E-cadherin throughout the entire genitalia (Figure 3A). In
165 contrast with the adjacent tissues, F-actin is also concentrated along the apico-basal axis of
166 posterior lobe cells (Figure 3A). This F-actin localization was unique to the posterior lobe, as it is
167 less intense in neighboring structures, such as the lateral plate, clasper, and sheath, as well as
168 in non-lobed species (Figure 3A; Figure 3 - supplement 1). Next we evaluated microtubules by
169 examining two post-translational modifications that appear on tubulin, acetylation of α -tubulin on
170 lysine40, a stabilizing modification (Roll-Mecak, 2019; Xu et al., 2017), and tyrosinated tubulin,
171 which has been associated with rapid microtubule turnover (Roll-Mecak, 2019; Webster,
172 Gundersen et al., 1987). In the posterior lobe, acetylated tubulin levels are highest at the apex
173 (top of the image) of the posterior lobe and weaken towards the basal side of the lobe (Figure
174 3B-C). Compared to other structures in the genitalia, acetylated tubulin is greatly increased
175 specifically in the posterior lobe (Figure 3B-C). In contrast, the levels of acetylated tubulin in
176 non-lobed species are similar throughout the genitalia (Figure 3 - supplement 1). We found
177 tyrosinated tubulin has a more consistent signal along the entire apico-basal axis in the
178 posterior lobe (Figure 3B&D). The amount of tyrosinated tubulin in posterior lobe cells is
179 increased compared to neighboring structures, but is weaker relative to the observed
180 differences in acetylated tubulin. In non-lobed species the levels of tyrosinated tubulin are
181 consistent across the entire genitalia (Figure 3- supplement 1). Collectively, these results
182 suggest that changes in assembly and/or dynamics of both F-actin and microtubule cytoskeletal
183 networks could be contributing factors in changing the shape of posterior lobe cells to increase
184 its height along the apico-basal axis.

185

186 **An apical extracellular matrix associates with posterior lobe cells**

187 In addition to investigating cell autonomous mechanisms leading to increases in tissue
188 thickness, we also sought to identify sources of external forces which could play a role in
189 posterior lobe morphogenesis. Such an external role for ECM during *Drosophila* pupal
190 development has been established in the wing of *D. melanogaster*, where decreases in both the
191 basal and apical ECM are needed for tissue elongation during early development (Diaz-de-la-

192 Loza et al., 2018), but during later developmental time periods the aECM serves an additional
193 role in shaping the wing by tethering cells to the overlying pupal cuticle (Etournay et al., 2015;
194 Ray et al., 2015). We first attempted to characterize the basal ECM by analyzing a GFP-tagged
195 version of Collagen IV (Viking:GFP). We observed that Viking:GFP, while present at very early
196 stages of genital morphogenesis, is weakly present during posterior lobe formation across the
197 entire genitalia (Figure 4 - supplement 1), suggesting that minimal basal ECM is present at this
198 time point. To further test for the presence of basal ECM we examined another basal ECM
199 component, Perlecan (Pcan:GFP) and also observed weak signal. Together, this data suggests
200 that the basal ECM is globally decreased in the genitalia during early pupal development, such
201 that it is very weak during posterior lobe morphogenesis.

202

203 We next sought to determine if an apical ECM is present, and if so, whether it could potentially
204 influence posterior lobe morphogenesis. A major component of the aECM is Dumpy (Dumpy),
205 which encodes a gigantic (2.5 MDa) zona pellucida domain-containing glycoprotein (Wilkin et
206 al., 2000). We examined a line in which Dumpy is endogenously tagged with a Yellow
207 Fluorescent Protein (Dumpy:YFP). Dumpy:YFP forms a complex three-dimensional network
208 over the pupal genitalia and is closely associated with cells of the posterior lobe (Figure 4;
209 Figure 4 - video 1). At certain points in the genitalia, this aECM network of Dumpy can extend
210 up to 39.4 μm on average above the cells, which is taller than the thickness of posterior lobe
211 cells at the beginning of development (Figure 4 - supplement 2). The intricate complex
212 morphology of this aECM network is hard to fully appreciate in flattened images due to its three-
213 dimensional shape and spatially varying levels of Dumpy:YFP, making it difficult to see weaker
214 populations of Dumpy without over-saturating more concentrated deposits.

215

216 In late pupal wing development, Dumpy anchors the wing to the surrounding cuticle, preventing
217 the tissue from retracting away from the cuticle, which is important to properly shape the wing
218 (Etournay et al., 2015; Ray et al., 2015). This same mechanism has been hypothesized to also
219 occur in the leg and antennae, however, in the posterior lobe we do not find discrete anchorage
220 points to the cuticle. Instead, we observed a large tether of Dumpy emanating from the anal
221 plate and connecting with the pupal cuticle membrane that encases the entire pupa (Figure 4 -
222 supplement 3, video 2) (Bainbridge & Bownes, 1981). This tether does not come in direct
223 contact with posterior lobe associated Dumpy or other nearby structures such as the lateral
224 plate, clasper, sheath, or phallus, suggesting that if Dumpy is contributing to posterior lobe

225 evolution and morphogenesis, it is likely through a mechanism which does not depend on a
226 direct mechanical linkage with the overlying pupal cuticle.

227
228 To investigate the role that Dumpy may play in posterior lobe morphogenesis, we examined its
229 localization throughout development. Prior to posterior lobe development, future cells of the lobe
230 lack apical Dumpy, and yet an intricate network associated with the clasper is observed (Figure
231 4A). However, from the early stages of posterior lobe development, as it first protrudes from the
232 lateral plate, we observe large deposits of Dumpy associated with future lobe cells (Figure 4B).
233 These deposits persist throughout most of its development (Figure 4C), becoming more
234 restricted to the apex of the posterior lobe towards the end of posterior lobe development
235 (Figure 4D). Throughout development the posterior lobe associated Dumpy population is
236 connected to the complex network of Dumpy associated with more medial structures such as
237 the phallus (Figure 4 A2-D2), indicating that the posterior lobe is interconnected via the aECM
238 with nearby structures (Figure 4). In contrast to the posterior lobe, the lateral plate has minimal
239 Dumpy associated with it (Fig. 4). Only when we oversaturate the Dumpy:YFP signal can we
240 observe a weak population of Dumpy associated with the lateral plate (Figure 4 - supplement 4).
241 Together, this indicates that the cells of the posterior lobe and the lateral plate substantially
242 differ in the levels of associated Dumpy, suggesting a potential role in the morphogenesis of the
243 posterior lobe.

244

245 **Expansion of Dumpy expression is correlated with the evolution of the posterior** 246 **lobe**

247 The association of the posterior lobe with Dumpy suggests that changes in the expression of
248 *dumpy* may have been significant during the evolution of the posterior lobe. To test if posterior
249 lobe-associated Dumpy is a unique feature of species which produce a posterior lobe, we
250 compared the spatial distribution of its mRNA in *D. melanogaster* with *D. biarmipes*, a species
251 which lacks this structure. Early in pupal genital development at 28 to 32 hours APF we observe
252 very similar expression patterns of *dumpy* between *D. melanogaster* and *D. biarmipes*, with
253 expression at the base of the presumptive lateral plate-clasper (Figure 5A-B, Figure 5 -
254 supplement 1). From 36 to 40 hours APF, when the posterior lobe begins to develop, this
255 pattern becomes restricted to a small region at the base of the lateral plate and clasper, near
256 the anal plate in *D. biarmipes*, but is expanded in lobed species (Figure 5A-B, Figure 5 -
257 supplement 1). By 44 hours APF expression of *dumpy* is reduced in the posterior lobe, as well

258 as in non-lobed species, with strongest expression associated with the clasper in *D. biarmipes*
259 (Figure 5A-B, Figure 5 - supplement 1). Overall, these results indicate that expression of *dumpy*
260 is expanded in a lobed species and correlates with the timing of the posterior lobe's formation.
261 In addition, considering that the developmental timing of *D. biarmipes* lags behind *D.*
262 *melanogaster* by approximately 4 hours (Figure 1 - supplement 1), this suggests that *dumpy*
263 expression becomes restricted during an earlier developmental period in the non-lobed species
264 *D. biarmipes*.

265
266 Although, it appears that the expression of *dumpy* has expanded in *D. melanogaster*, Dumpy is
267 an extracellular protein, and cells expressing its mRNA may not correlate with its ultimate
268 protein abundance or localization. Since an antibody for Dumpy is not available, we adapted
269 lectin staining protocols which can detect glycosylated proteins like Dumpy in order to compare
270 the distribution of aECM in species which lack posterior lobes. We found that fluorescein
271 conjugated *Vicia villosa* lectin (VVA), which labels *N*-acetylgalactosamine (Tian & Ten Hagen,
272 2007), approximately recapitulated Dumpy:YFP in *D. melanogaster*. VVA strongly associates
273 with the posterior lobe, shows trace association with the lateral plate, and roughly mirrors the
274 complex three-dimensional shape of the Dumpy aECM network covering the center of the
275 genitalia (Figure 5C). When we examined VVA in the non-lobed species *D. biarmipes*, we found
276 VVA labeled a weak strand-like structure emanating from the clasper and connecting to the
277 crevice between the lateral plate and clasper where the presumptive posterior lobe would form
278 (Figure 5D). In addition to this, we also observed a weak connection to the tip of the lateral
279 plate, similar to what is observed on the lateral plate of lobed species (Figure 5D). We also
280 observed strong VVA signal over the center of the genitalia in *D. biarmipes*, similar to what we
281 observe in *D. melanogaster* (Figure 5 C-D). These results correlate with our *in situ* results,
282 where we observe high expression at the center of the genitalia and weak expression of *dumpy*
283 at the base between the clasper and lateral plate in *D. biarmipes*, which may be responsible for
284 forming the weak aECM connection from the clasper to the crevice. Further, we found only a
285 very weak aECM signal in an additional non-lobed species, *D. ananassae* (Figure 5 -
286 supplement 2), covering the equivalent cells that would form a posterior lobe. Collectively, these
287 data suggest that an ancestral aECM network was associated with the central genital structures,
288 including the phallus, sheath, and clasper, and a weak association in the crevice next to
289 prospective posterior lobe cells. During the course of evolution, expression of *dumpy* has
290 expanded to integrate cells of the posterior lobe, creating a prominent connection to the aECM
291 network.

292

293 **Dumpy is required for proper posterior lobe formation**

294 Thus far, we observed a strong association of the aECM with cells that form the posterior lobe,
295 a trait which is much less pronounced in non-lobed species. To determine if Dumpy plays a role
296 in posterior lobe formation we next employed transgenic RNAi to knock down its expression.
297 Previous studies of *dumpy* characterized a VDRC RNAi line that is effective at reducing its
298 function (Ray et al., 2015). We used a driver from the *Pox neuro* gene (Boll & Noll, 2002) to
299 reduce *dumpy* levels in the posterior lobe. This resulted in a drastic decrease in the size and
300 shape of the posterior lobe compared to a control RNAi (Figure 6A,C). In *dumpy* knockdown
301 individuals, we observe a variable phenotype, and even within single individuals, the severity of
302 phenotype differs between left and right posterior lobes (Figure 6A; Figure 6 -supplement 1).
303 Knockdown was completed at both 25°C and 29°C, as higher temperatures increase the
304 efficacy of the Gal4/UAS system (Duffy, 2002). At higher temperatures, the *dumpy* knockdown
305 phenotype trended towards more severe defects (Figure 6B). Together, the reduction in lobe
306 size and shape variation with *dumpy* knockdown suggests that posterior lobe development is
307 sensitive to levels of *dumpy*, and that *dumpy* plays a vital role in shaping the posterior lobe.

308

309 **Correlation of Dumpy deposition and cell height in the posterior lobe**

310 We next sought to determine when during development *dumpy* knockdown influences the
311 morphogenetic progression of the posterior lobe. This was important because we observed both
312 a slow and a fast phase of lobe development (Figure 1F), and also reasoned that posterior lobe
313 cells secrete cuticle once they have adopted their final adult conformations, of which any of
314 these phases could represent a critical Dumpy-dependent stage of development. We found that
315 *dumpy* knockdown individuals manifest phenotypes very early on (Figure 7A) and continue to
316 show abnormal lobe development through the end of its formation (Figure 7B). Interestingly,
317 differences in the height of cells on the ventral side of the posterior lobe are not observed
318 between control and *dumpy* knockdown treatments, instead defects in cell height are observed
319 in the more dorsally-localized cells of the posterior lobe (Figure 7A-B). This correlates with the
320 phenotypes of the adults in the *dumpy* knockdown in which the ventral tip is of normal height
321 with defects observed towards the dorsal side (Figure 6A). However, this phenotype appears
322 counterintuitive, as Dumpy protein normally associates along the entire posterior lobe, so why
323 does the tip of the posterior lobe develop to normal height when Dumpy is absent? To better
324 understand this phenotype, we examined Dumpy:YFP localization in the *dumpy* knockdown

325 background. We observed a weak association of Dumpy with the ventral cells of the posterior
326 lobe both in early (Figure 7D n=5/5 samples) and late (Figure 7F n=4/5 samples) stages
327 compared to control samples. The fact that one of the samples have Dumpy associated with the
328 ventral side of the lobe correlates with our observation that not all adult samples are fully
329 extended on the ventral side (Figure 7 - supplement 1) suggesting that the association with
330 Dumpy may be lost late in development, leading to shortening of these cells. In addition, we
331 observed more severe phenotypes in *dumpy* knockdown with the *dumpy-yfp background*
332 (compared to the *dumpy* WT *dumpy* background alone), suggesting that Dumpy:YFP is a mild
333 hypomorph. In both early and late (Figure 7D & F) samples, no association between
334 Dumpy:YFP and the dorsal side of the posterior lobe was observed. However, at early time
335 points random strands can be observed in the middle of the lobe (between the tip and base), but
336 these varied from sample to sample (Figure 7 -supplement 2) These strands visually resembled
337 the strands of VVA observed in *D. biarmipes* (Figure 5D), in that they emanate from the clasper
338 and connect to the crevice between the posterior lobe and clasper. Overall, these results
339 suggest that sporadic residual Dumpy:YFP localization in the *dumpy* knockdown is responsible
340 for the variable nature of the adult phenotypes we observed. The most pronounced phenotypic
341 defects manifest in regions with the strongest reduction in Dumpy aECM deposition, implying
342 that Dumpy's presence is required for posterior lobe cells to elongate and project from the
343 lateral plate.

344

345 **Discussion**

346 Here, we determined how a morphological novelty forms at the cellular level, and in doing so,
347 revealed distinctive cell and aECM interactions underlying its development and evolution. We
348 identified how an extreme change in the shape of cells in the developing posterior lobe accounts
349 for its novel morphology. While intrinsic cytoskeletal components may contribute to this process,
350 our results highlight the critical role played by a vast extrinsic network of ECM on the apical side
351 of the epithelium. It was unexpected that such an elaborate supercellular matrix structure would
352 participate in the evolution of a seemingly simple novelty. Below, we consider the potential roles
353 played by the aECM in posterior lobe development and diversification, and discuss how studies
354 of morphogenesis can illuminate the simple origins of structures that might otherwise seem
355 impossibly complex to evolve.

356

357 **Mechanisms for aECM-mediated control of cell height in the posterior lobe**

358 Our work demonstrates an important role for the aECM protein, Dumpy, in the growth of the
359 posterior lobe, as exhibited by the dramatic phenotypes in the *dumpy* RNAi background and the
360 strong association of Dumpy:YFP with only the tallest cells in these experiments. Our data is
361 consistent with three possible mechanisms. First, Dumpy could serve as a structural support
362 while autonomous cell mechanical processes drive apico-basal elongation. Second, the cells of
363 the posterior lobe could be pulled mechanically through their connection to the Dumpy aECM.
364 This process could operate passively, deforming cells of the lobe, but could also drive changes
365 in the cytoskeleton in response to external tensions. Finally, the aECM could play a direct role
366 by signaling through lobe cells, as has been exhibited by the basal ECM (Kirkpatrick et al.,
367 2004; Kreuger et al., 2004; Wang et al., 2008). Previous research has shown that the JAK/STAT
368 pathway is important for posterior lobe development (Glassford et al., 2015), and their ability to
369 signal to the correct cells could be altered in the absence of Dumpy. Of course, these models
370 are not mutually exclusive and some combination of these mechanisms may be integrated to
371 shape the posterior lobe. Our observations of increased cytoskeletal components in posterior
372 lobe cells and the reduced height of cells that lack Dumpy in our knockdown experiments are
373 consistent with all three mechanisms, which are difficult to differentiate experimentally. When
374 we examine morphogenesis in non-lobed species, we observed that the lateral plate drops
375 below the clasper (Figure 1 - supplement 1). Assuming this ancestral process still occurs in
376 lobed species, it is quite possible that the aECM ‘holds’ cells of the posterior lobe during the
377 early stages of posterior lobe development while the lateral plate is pulled down, causing them
378 to elongate to relieve the stress. Future manipulative biomechanical studies will be required to
379 explore these possibilities.

380

381 **The role of aECM in the diversification of genital structures**

382 Genitalia represent some of the most rapidly diversifying structures in the animal kingdom, and
383 our results suggest the aECM may participate in the modification of *Drosophila* genital
384 structures. The shape of the posterior lobe is extremely diverse among species of the
385 *melanogaster* clade (Coyne, 1993). Our results demonstrate that reducing the levels of Dumpy
386 can affect the shape of the posterior lobe, with extreme knockdown phenotypes approximating
387 the posterior lobe of *D. mauritiana*. Furthermore, the clasper and phallus show dense deposits
388 of Dumpy, suggesting that the aECM could play important roles in diversifying these remarkably
389 variable structures. During the course of evolution one could imagine that by altering which cells

390 are connected to the aECM, the strength of those connections, or the forces acting on those
391 connections could lead to changes in morphological shape. Hence identifying causative genes
392 that differentiate these structures could uncover novel mechanisms for genetically controlling
393 the behavior of this aECM and behaviors of cells bound to this dynamic scaffold.

394

395 **Integrating cells into a pre-existing aECM network to generate morphological** 396 **novelty**

397 In comparing the morphogenesis of a novel structure to close relatives which lack it
398 (representing a proxy for the ancestral state), we identified a likely path by which the aECM
399 became associated with the posterior lobe. The aECM, while understudied, has been implicated
400 in the morphogenesis of many structures ([Diaz-de-la-Loza et al., 2018](#); [Etournay et al., 2015](#);
401 [Ray et al., 2015](#); [Fernandes et al., 2010](#); [Dong et al., 2014](#); [Mancuso et al., 2012](#)), and yet, its
402 role during the evolution of novel structures is largely unexplored. We find a conserved aECM
403 network associated with central genital structures (clasper, sheath, and phallus) in both lobed
404 and non-lobed species. In non-lobed species, *dumpy* is expressed weakly at the base between
405 the lateral plate and clasper resulting in a thin connection of aECM from clasper to the crevice
406 (Figure 8). By contrast, lobed species express high levels of *dumpy* between the presumptive
407 posterior lobe and clasper, resulting in large amounts of aECM in the crevice. We hypothesize
408 that this increase in aECM allows cells at the base of the lateral plate to be integrated into this
409 ancestral aECM network (Figure 8), a step which was likely significant to its evolution. Overall,
410 this suggests that the aECM could be an unexpected target for generating novel anatomical
411 structures.

412

413 The expanded *dumpy* expression we observed caused us to consider how the posterior lobe
414 gained this aECM attachment. Interestingly, our previous work found a gene regulatory network
415 (GRN) that regulates development of an ancestral embryonic structure, the posterior spiracles,
416 was co-opted during the evolution of the posterior lobe and regulates its development
417 ([Glassford et al., 2015](#)). Previous work has shown that *dumpy* is expressed in the posterior
418 spiracles ([Wilkin et al., 2000](#)), and we have observed a thin tether of Dumpy:YFP connecting the
419 posterior spiracles to the surrounding embryonic cuticle (Figure 8 Supplement 1). This is
420 consistent with previously identified roles for Dumpy in epithelia-cuticle attachment in the wing
421 ([Etournay et al., 2015](#); [Ray et al., 2015](#)) and hypothesized role in the muscle, leg, and antenna
422 ([Wilkin et al., 2000](#); [Ray et al., 2015](#)). Identification of regulatory elements which activate *dumpy*

423 in the posterior lobe will be necessary to determine whether it's role in the posterior spiracle was
424 relevant to the evolution of expanded genital expression.

425
426 Evolution is thought to act through the path of least resistance. When confronted with the
427 remarkable diversity of genital morphologies present in insects, one must wonder how the
428 intricate projections, bumps, and divots form in its underlying epithelia. Models of co-option have
429 been appealing because they establish pre-existing mechanisms in place that can be rapidly
430 ported to new locations to generate massive changes in a tissue. Our examination of the cellular
431 processes during posterior lobe morphogenesis highlights a different way that co-option may
432 work. Here, the aECM mechanism we uncovered appears to be a path of least resistance
433 because this tissue already uses a vast network of aECM to potentially pattern other structures,
434 such as the phallus and its multiple elaborations. Because this network of aECM represents a
435 pre-existing condition, it is easy to appreciate how cells of the posterior lobe could evolve novel
436 extracellular connections to this network to generate a new protrusion. On the other hand,
437 tissues which lack such an ancestral network may well be less likely to evolve projections
438 through this mechanism. While the aECM is required for this morphogenetic process, we
439 envision that additional networks and processes must be contributing to the full morphogenesis
440 of the posterior lobe. Determining genetic changes which underlie such remarkable cellular
441 responses represents a major looming challenge in evo-devo research (Smith, Rebeiz, &
442 Davidson, 2018).

443

444 **Materials and Methods**

445

446 **Key resources table**

447

Reagent type (species) or resource	Designation	Source or reference	Identifiers	Additional Information
Antibody	rat anti-alpha tubulin (tyrosinated)	MilliporeSigma	Millipore Cat# MAB1864-I	IHC (1:500)
Antibody	mouse anti-alpha tubulin (acetylated)	Sigma-Aldrich	Sigma-Aldrich Cat# T6793, RRID:AB_477585	IHC (1:500)

Antibody	rat anti-Ecadherin	DSHB	DSHB Cat# DCAD2, RRID:AB_528120	IHC (1:500)
Antibody	mouse anti-fasciclin III	DSHB	DSHB Cat# 7G10 anti-Fasciclin III, RRID:AB_528238	IHC (1:500)
Antibody	rabbit anti-histone H3 (phospho S10)	Abcam	Abcam Cat# ab5176, RRID:AB_304763	IHC (1:50)
Antibody	goat anti-GFP	Abcam	Abcam Cat# ab6662, RRID:AB_305635	IHC (1:300)
Antibody	fluorescein Vicia Villosa Lectin (VVA)	Vector Laboratories	Vector Laboratories Cat# FL-1231, RRID:AB_2336856	IHC (1:200)
Chemical compound, drug	rhodamine phalloidin	Thermo Fisher Scientific	Thermo Fisher Scientific Cat# R415, RRID:AB_2572408	IHC (1:200)
Strain, strain background (<i>Drosophila melanogaster</i>)	<i>y¹w¹ Drosophila melanogaster</i>	Bloomington Drosophila Stock Center	BDSC Cat# 1495, RRID:BDSC_1495	
Strain, strain background (<i>Drosophila biarmipes</i>)	wild type	National Drosophila Species Stock Center (NDSSC)	NDSSC Stock #: 14023-0361.10 RRID:FlyBase_FBst0203870	
Strain, strain background (<i>Drosophila ananassae</i>)	wild type	National Drosophila Species Stock Center (NDSSC)	NDSSC Stock #: 14024-0371.13 RRID:FlyBase_FBst0201380	No longer available
Strain, strain background (<i>Drosophila pseudoobscura</i>)	wild type	National Drosophila Species Stock Center (NDSSC)	NDSSC Stock #: 14011-0121.87 RRID:FlyBase_FBst0200074	No longer available
Genetic reagent (<i>Drosophila melanogaster</i>)	<i>UAS-Raeppli-CAAX</i>	Bloomington Drosophila Stock Center (BDSC)	BDSC Cat# 55084, RRID:BDSC_55084	
Genetic reagent	<i>pox neuro-Gal4</i>	(Boll & Noll, 2002)	Construct #13	

<i>(Drosophila melanogaster)</i>				
Genetic reagent <i>(Drosophila melanogaster)</i>	<i>D. simulans</i> <i>pox neuro-Gal4</i>	This paper	N/A	
Genetic reagent <i>(Drosophila melanogaster)</i>	hs – flippase ¹²²	Gift from Erika A. Bach	Flybase: FBtp0001101	
Genetic reagent <i>(Drosophila melanogaster)</i>	<i>armadillo-GFP</i>	Bloomington Drosophila stock center	BDSC Cat# 8556, RRID:BDSC_8556	
Genetic reagent <i>(Drosophila melanogaster)</i>	Dumpy:YFP	Drosophila Genomics and Genetic Resources	DGGR Cat# 115238, RRID:DGGR_115 238	
Genetic reagent <i>(Drosophila melanogaster)</i>	E-cadherin:mCherry	Bloomington Drosophila stock center	BDSC Cat# 59014, RRID:BDSC_5901 4	
Genetic reagent <i>(Drosophila melanogaster)</i>	<i>UAS-dumpyRNAi</i>	Vienna Drosophila Resource Center	VDRC Cat#44029, RRID:FlyBase_FB st0465370	
Genetic reagent <i>(Drosophila melanogaster)</i>	<i>UAS-mCherryRNAi</i>	Bloomington Drosophila stock center	BDSC Cat# 35785, RRID:BDSC_3578 5	
Recombinant DNA reagent	pS3aG4	Gift from Benjamin Prud'homme	N/A	Gal4 vector used to make <i>D. simulans</i> <i>pox neuro gal4</i> line
Sequence-based reagent	GCCACTAACAAAT CCATGCGGTT	This paper	N/A	<i>dumpy</i> probe forward primer
Sequence-based reagent	TAATACGACTCA CTATAGGGAGA AATAGCCCTGTC CTTGGAATCC	This paper	N/A	<i>dumpy</i> probe reverse primer with T7 primer
Sequence-based reagent	TTCCGGGCGCG CCTCGGTGGCT TAACACGCGCAT T	This paper	N/A	<i>D. simulans</i> <i>pox neuro</i> forward primer for gal 4 line
Sequence-based reagent	TTGCCCTGCA GGATCGCTGATT CCATGGCCCAG	This paper	N/A	<i>D. simulans</i> <i>pox neuro</i> reverse primer for gal 4

	T			line
Software algorithm	Fiji (ImageJ v2.0)	(Schindelin et al., 2012)	RRID:SCR_002285	
Software algorithm	GenePalette	(Rebeiz & Posakony, 2004)	N/A	
Software algorithm	Microsoft Excel	Microsoft	RRID:SCR_016137	
Software algorithm	MorphoGraphX	(Barbier de Reuille et al., 2015)	N/A	
Software algorithm	Prism 8	GraphPad	N/A	

448

449

450 Fly stocks and genetics

451 Fly stocks were reared using standard culture conditions. Wild type species used in this study
452 were obtained from the University of California, San Diego *Drosophila* Stock Center (now known
453 as The National Drosophila Species Stock Center at Cornell University)(*Drosophila biarmipes*
454 #14024-0361.10, *Drosophila ananassae* #14024-0371.13, *Drosophila pseudoobscura* #14011-
455 0121.87) and from the Bloomington Drosophila Stock Center (*Drosophila melanogaster* [y^1w^1]
456 #1495). *pox neuro-Gal4* (construct #13) was obtained from Werner Boll (Boll & Noll, 2002). The
457 following were obtained from the Bloomington Drosophila stock center: *UAS-Raepli-CAAX*
458 (#55084), *armadillo-GFP* (#8556), *Ecadherin:mCherry* (#59014), and *UAS-mCherryRNAi*
459 (control for RNAi experiments, as mCherry is not a gene in the *Drosophila* genome)(35785).
460 *UAS-dumpyRNAi* was obtained from the Vienna Drosophila Resource Center (#44029) and
461 *Dumpy:YFP* was obtained from the Drosophila Genomics and Genetic Resources (#115238).

462

463 For the Raepli experiments, stable lines of *hs-flippase*; *UAS-Raepli-CAAX/UAS-Raepli-*
464 *CAAX* and *D. simulans pox neuro-gal4/D. simulans pox neuro-gal4;UAS-Raepli-CAAX/UAS-*
465 *Raepli-CAAX* were generated. *D. simulans pox neuro-gal4* was used as opposed to *pox neuro-*
466 *gal4* because a *gal4* driver on the second chromosome was required. Virgin females from the
467 first line were crossed to males from the second line to ensure *hs-flippase* was in all offspring.
468 Offspring were collected and grown as normal, heat shocked at 37°C for 1 hour around 24 to 28
469 hours APF, and allowed to finish development at 25°C.

470

471 Sample Preparation

472 Pupal samples were prepared following protocol in Glassford, et al., 2015. Briefly, samples were
473 incubated at 25°C unless otherwise noted. Dissections were performed in cold PBS, pupae
474 were cut in half, removed from pupal case, and fat bodies removed by flushing. Larval samples
475 were dissected in cold PBS by cutting the larva in half and flipping the posterior end of the larval
476 inside out. All samples were fixed for 30 minutes at room temperature in PBS with 0.1% Triton-X
477 and 4% paraformaldehyde. Samples stained with phalloidin had Triton-X concentrations
478 increased to 0.3%. Samples used for VVA stain were removed from pupal cuticle before being
479 fixed in PBS with 0.1% Triton-x, 4% paraformaldehyde, and 1% trichloroacetic acid on ice for 1
480 hour followed by 30 minutes at room temperature. This method causes some slight tissue
481 distortion, as the precipitation treatment utilized to refine the VVA signal causes the posterior
482 lobe to become slightly deformed and curve in towards the clasper. However, similar defects
483 were not observed in the other structures such as the lateral plate or in *D. biarmipes*. Samples
484 were stored in PBT for immunostaining at 4°C up to 2 days. For *in situ* hybridization, samples
485 were rinsed twice in methanol and rinsed twice in ethanol. Samples were stored at -20°C in
486 ethanol.

487

488 **Immunostaining and *in situ* hybridization**

489 Genital samples were removed from the surrounding pupal cuticle and incubated overnight at
490 4°C with primary antibodies diluted in PBS with 0.1% Triton-X (PBT). VVA and phalloidin
491 samples were placed on a rocker. The following primary antibodies were used: rat anti-alpha
492 tubulin (tyrosinated) 1:500 (MAB 1864-I, MilliporeSigma), mouse anti-alpha tubulin (acetylated)
493 1:500 (T6793, Sigma-Aldrich), rat anti-Ecadherin 1:500 (DCAD2, DSHB), mouse anti-fasciclin III
494 1:500 (7G10, DSHB), rabbit anti-histone H3 (phospho S10) 1:50 (ab5176, Abcam), goat anti-
495 GFP 1:300 (ab6662, Abcam), fluorescein Vicia Villosa Lectin (VVA) 1:200 (FL-1231, Vector
496 Laboratories). The goat anti-GFP was used to increase signal of DumpY:YFP in the knockdown
497 experiments only. Primary antibody was removed by performing two quick rinses and two long
498 washes (at least 5 minutes) in PBT. Samples were incubated overnight at 4°C in secondary
499 antibodies diluted in PBT. The following secondary antibodies were used: donkey anti-rat Alexa
500 594 1:500 (A21209, Invitrogen), donkey anti-mouse Alexa 488 1:500 (A21202, Thermo Fisher
501 Scientific), donkey anti-rat Alexa 488 1:500 (A21208, Thermo Fisher Scientific), goat anti-mouse
502 Alexa 594 1:500 (A-11005, Thermo Fisher Scientific), goat anti-rabbit Alexa 594 1:500 (A-
503 11012, Thermo Fisher Scientific), donkey anti-goat Cy2 1:500 (705-225-147, Jackson
504 ImmunoResearch). Rhodamine phalloidin (R415, Thermo Fisher Scientific) stain was performed
505 with secondary antibody Samples were washed out of secondary antibody by performing two

506 quick rinses and two long washes (at least 5 minutes) in PBT. Samples were then incubated in
507 50% PBT/50% glycerol solution for at least 5 minutes. Pupal samples were mounted on glass
508 slides coated with Poly-L-Lysine Solution in an. Glass slides had 1 to 2 layers of double side
509 tape with a well cut out in which the sample was placed and covered with a cover slip. Larval
510 samples were placed on a slide with an 80% glycerol 0.1M Tris-HCL (pH 8.0) solution, genital
511 disc was separated from larva carcass at this time and larva carcass removed. A glass cover
512 slip was then placed onto of the discs (without doubled sided tape).

513

514 *in situ* hybridization was performed following the protocol in Rebeiz et al., 2009 with
515 modifications to perform *in situs* in the InsituPro VSi robot (Intavis Bioanalytical Instruments) as
516 done by Glassford et al., 2015.

517

518 **Microscopy and live imaging**

519 Cuticles of adult posterior lobes and *in situ* hybridization samples were imaged on Leica
520 DM2000 with a 40x objective for cuticles and a 10x objective for *in situ* samples. Samples with
521 fluorescent antibodies and fluorescently tagged proteins were imaged using a Leica TCS SP5
522 Confocal microscope using either a 40x or 63x oil immersion objective.

523

524 To live image genital development, a 2% agar solution was poured into a small petri dish filling
525 the dish half way. A 0.1-10 μ L pipette tip was used to make small wells in the agar for pupal
526 samples. Timed out pupal samples were inserted head first into the small well and a 5-300 μ L
527 pipette tip was used to push sample into agar by placing the tip around the posterior spiracles
528 on the pupal case. To better image the developing genitalia the pupal case at the posterior end
529 was removed with forceps. Deionized water was used to cover the samples and imaged on a
530 Leica TCS SP5 Confocal microscope using a 63x water objective.

531

532 To live image embryos, Dumpy:YFP flies were grown in egg-laying chamber with grape agar
533 plates (Genesee Scientific). Embryos were removed from plates using forceps and rolled on a
534 piece of double sided tape to remove the chorion. Embryos then were positioned on a glass
535 coverslip coated with embryo glue. A glass slide was covered with double sided tape and a well
536 was made and filled with halocarbon 27 oil. The cover slip with the embryos was then placed on
537 the glass slide, submerging the embryos in halocarbon oil. Embryos were imaged on a Leica
538 TCS SP8 confocal with a 63x oil objective.

539

540 **Image analysis**

541 Images were processed with Fiji (Schindelin et al., 2012) and Photoshop. Three-dimensional
542 views were completed in MorphoGraphX (Barbier de Reuille et al., 2015). Movies were
543 processed in Fiji and cell rearrangements were tracked using the manual tracking plugin. Tissue
544 thickness/cell height during development was measured in cross-section view by drawing a line
545 centered between the two sides (based on apical membrane) of the lobe until the basal side
546 was reached. Area of adult posterior lobe cuticles and height of the adult lobe were measured
547 by using the lateral plate as a guide for determining the bottom boundary of the posterior lobe.
548 To prevent any possible bias for one lobe vs the other (i.e. left vs right) which lobe was used in
549 statistical analysis was randomly decided, except for Figure 6 - supplement 1 where both sides
550 of the posterior lobe were considered.

551

552 **Transgenic Construct**

553 To make the *D. simulans* *pox neuro-gal4* driver, the posterior lobe enhancer for *pox neuro* in *D.*
554 *simulans* identified in Glassford et al., 2015 was cloned using primers listed in key resources
555 table using genomic DNA purified with the DNeasy Blood and Tissue Kit (QIAGEN). Primers
556 were designed using sequence conservation with the GenePalette software tool (Rebeiz and
557 Posakony 2004; Smith et al., 2017). The cloned sequence was inserted into the pS3aG4 (Gal4)
558 using *AscI* and *SbfI* restriction sites. The final construct was inserted into the 51D landing site
559 on the second chromosome (Bischof et al., 2007).

560

561 **Acknowledgements**

562
563 The authors thank the members of the M.R. laboratory for comments and discussion on the
564 manuscript. We thank Werner Boll and Markus Noll for the *pox neuro-gal4* line, the Bloomington
565 stock center, VDRC, and DGGR stock centers for fly stocks, Benjamin Prud'homme for the
566 s3aG4 vector, Erika A. Bach for the hs-flippase line, and Winslow Johnson for the *D. simulans*
567 *pox neuro-gal4* line. This work was supported by the National Institutes of Health (GM107387 to
568 M.R. and HD044750 to L.A.D.).

569

570 **Author details**

571

572 Sarah Jacquelyn Smith
573 Department of Biological Sciences, University of Pittsburgh
574 Contributions: Conceptualization, Methodology, Validation, Formal analysis, Investigation, Data
575 curation, Writing-original draft, Writing-review and editing, Visualization
576 Competing interests: No competing interests declared
577 ORCID: 0000-0002-1469-1821
578
579 Lance A. Davidson
580 Department of Bioengineering University of Pittsburgh
581 Contributions: Conceptualization, Methodology, Writing-review and editing, Funding acquisition
582 Competing interests: No competing interests declared
583 ORCID: 0000-0002-2956-0437
584
585 Mark Rebeiz
586 Department of Biological Sciences, University of Pittsburgh
587 Contributions: Conceptualization, Methodology, Writing-review and editing, Supervision,
588 Funding acquisition
589 Competing interests: No competing interests declared
590 ORCID: 0000-0001-5731-5570

591

592 **References**

593

594 Atallah, J., Liu, N.H., Dennis, P., Hon, A., & Larsen, E.W. (2009). Developmental constraints
595 and convergent evolution in *Drosophila* sex comb formation. *Evolution & Development*,
596 11(2), 205–218. <https://doi.org/10.1111/j.1525-142X.2009.00320.x>

597 Bainbridge, S.P., & Bownes, M. (1981). Staging the metamorphosis of *Drosophila*
598 melanogaster. *Journal of Embryology and Experimental Morphology*, 66, 57–80.

599 Barbier de Reuille, P., Routier-Kierzkowska, A.L., Kierzkowski, D., Bassel, G.W., Schüpbach,
600 T., Tauriello, G., Bajpai, N., Strauss, S., Weber, A., Kiss, A., Burian, A., Hofhuis, H., Sapala,
601 A., Lipowczan, M., Heimlicher, M.B., Robinson, S., Bayer, E.M., Basler, K., Koumoutsakos,
602 P., Roeder, A.H., Aegerter-Wilmsen, T., Nakayama, N., Tsiantis, M., Hay, A., Kwiatkowska,
603 D., Xenarios, I., Kuhlemeier, C., Smith, R.S. (2015). MorphoGraphX: A platform for
604 quantifying morphogenesis in 4D. *eLife*, 4, 05864. <https://doi.org/10.7554/eLife.05864>

- 605 Bischof, J., Maeda, R.K., Hediger, M., Karch, F., & Basler, K. (2007). An optimized transgenesis
606 system for *Drosophila* using germ-line-specific phiC31 integrases. *Proceedings of the*
607 *National Academy of Sciences of the United States of America*, 104(9), 3312–3317.
- 608 Boll, W., & Noll, M. (2002). The *Drosophila* Pox neuro gene: control of male courtship behavior
609 and fertility as revealed by a complete dissection of all enhancers. *Development*, 129(24),
610 5667–5681. <https://doi.org/10.1242/dev.00157>
- 611 Brown, N.H. (2011). Extracellular matrix in development: insights from mechanisms conserved
612 between invertebrates and vertebrates. *Cold Spring Harbor Perspectives in Biology*, 3(12),
613 a005082. <https://doi.org/10.1101/cshperspect.a005082>
- 614 Coyne, J.A. (1993). The genetics of an isolating mechanism between two sibling species of
615 *Drosophila*. *Evolution*, 47(3), 778–788.
- 616 Daley, W.P., & Yamada, K.M. (2013). ECM-modulated cellular dynamics as a driving force for
617 tissue morphogenesis. *Current Opinion in Genetics & Development*, 23(4), 408–414.
618 <https://doi.org/10.1016/j.gde.2013.05.005>
- 619 Diaz-de-la-Loza, M.D., Ray, R.P., Ganguly, P.S., Alt, S., Davis, J.R., Hoppe, A., Tapon, N.,
620 Salbreux, G., & Thompson, B.J. (2018). Apical and basal matrix remodeling control epithelial
621 morphogenesis. *Developmental Cell*, 46(1), 23–39.e5.
622 <https://doi.org/10.1016/j.devcel.2018.06.006>
- 623 Dong, B., Hannezo, E., & Hayashi, S. (2014). Balance between apical membrane growth and
624 luminal matrix resistance determines epithelial tubule shape. *Cell Reports*, 7(4), 941–950.
625 <https://doi.org/10.1016/j.celrep.2014.03.066>
- 626 Duffy, J.B. (2002). GAL4 system in *Drosophila*: a fly geneticist's Swiss army knife. *Genesis*,
627 34(1–2), 1–15. <https://doi.org/10.1002/gene.10150>
- 628 Eberhard, W.G. (1985). *Sexual selection and animal genitalia*. Harvard University Press.
- 629 Etournay, R., Popović, M., Merkel, M., Nandi, A., Blasse, C., Aigouy, B., Brandl, H., Myers, G.,
630 Salbreux, G., Jülicher, F., Eaton, S. (2015). Interplay of cell dynamics and epithelial tension
631 during morphogenesis of the *Drosophila* pupal wing. *eLife*, 4, e07090.
632 <https://doi.org/10.7554/eLife.07090>
- 633 Fernandes, I., Chanut-Delalande, H., Ferrer, P., Latapie, Y., Waltzer, L., Affolter, M., Payre, F.,
634 & Plaza, S. (2010). Zona pellucida domain proteins remodel the apical compartment for
635 localized cell shape changes. *Developmental Cell*, 18(1), 64–76.
636 <https://doi.org/10.1016/j.devcel.2009.11.009>

- 637 Frazee, S.R., & Masly, J.P. (2015). Multiple sexual selection pressures drive the rapid evolution
638 of complex morphology in a male secondary genital structure. *Ecology and Evolution*, 5(19),
639 4437–4450. <https://doi.org/10.1002/ece3.1721>
- 640 Glassford, W.J., Johnson, W.C., Dall, N.R., Smith, S.J., Liu, Y., Boll, W., Noll, M., & Rebeiz, M.
641 (2015). Co-option of an Ancestral Hox-Regulated Network Underlies a Recently Evolved
642 Morphological Novelty. *Developmental Cell*, 34(5), 520–531.
643 <https://doi.org/10.1016/j.devcel.2015.08.005>
- 644 Green, J.E., Cavey, M., Médina Caturegli, E., Aigouy, B., Gompel, N., & Prud'homme, B.
645 (2019). Evolution of ovipositor length in *Drosophila suzukii* is driven by enhanced cell size
646 expansion and anisotropic tissue reorganization. *Current Biology*, 29(12), 2075–2082.
647 <https://doi.org/10.1016/j.cub.2019.05.020>
- 648 Guirao, B., & Bellaïche, Y. (2017). Biomechanics of cell rearrangements in *Drosophila*. *Current*
649 *Opinion in Cell Biology*, 48, 113–124. <https://doi.org/10.1016/j.ceb.2017.06.004>
- 650 Heisenberg, C.P., & Bellaïche, Y. (2013). Forces in tissue morphogenesis and patterning. *Cell*,
651 153(5), 948–962. <https://doi.org/10.1016/j.cell.2013.05.008>
- 652 Irvine, K.D., & Wieschaus, E. (1994). Cell intercalation during *Drosophila* germband extension
653 and its regulation by pair-rule segmentation genes. *Development*, 120(4), 827–841.
- 654 Jagadeeshan, S., & Singh, R.S. (2006). A time-sequence functional analysis of mating
655 behaviour and genital coupling in *Drosophila*: role of cryptic female choice and male sex-
656 drive in the evolution of male genitalia. *Journal of Evolutionary Biology*, 19(4), 1058–1070.
657 <https://doi.org/10.1111/j.1420-9101.2006.01099.x>
- 658 Kanca, O., Caussinus, E., Denes, A.S., Percival-Smith, A., & Affolter, M. (2014). Raeppli: a
659 whole-tissue labeling tool for live imaging of *Drosophila* development. *Development*, 141(2),
660 472–480. <https://doi.org/10.1242/dev.102913>
- 661 Kirkpatrick, C.A., Dimitroff, B.D., Rawson, J.M., & Selleck, S.B. (2004). Spatial regulation of
662 Wingless morphogen distribution and signaling by Dally-like protein. *Developmental Cell*,
663 7(4), 513–523. <https://doi.org/10.1016/j.devcel.2004.08.004>
- 664 Kopp, A., & True, J.R. (2002). Evolution of male sexual characters in the oriental *Drosophila*
665 *melanogaster* species group. *Evolution & Development*, 4(4), 278–291.
666 <https://doi.org/10.1046/j.1525-142X.2002.02017.x>
- 667 Kreuger, J., Perez, L., Giraldez, A.J., & Cohen, S.M. (2004). Opposing activities of Dally-like
668 glypican at high and low levels of Wingless morphogen activity. *Developmental Cell*, 7(4),
669 503–512. <https://doi.org/10.1016/j.devcel.2004.08.005>

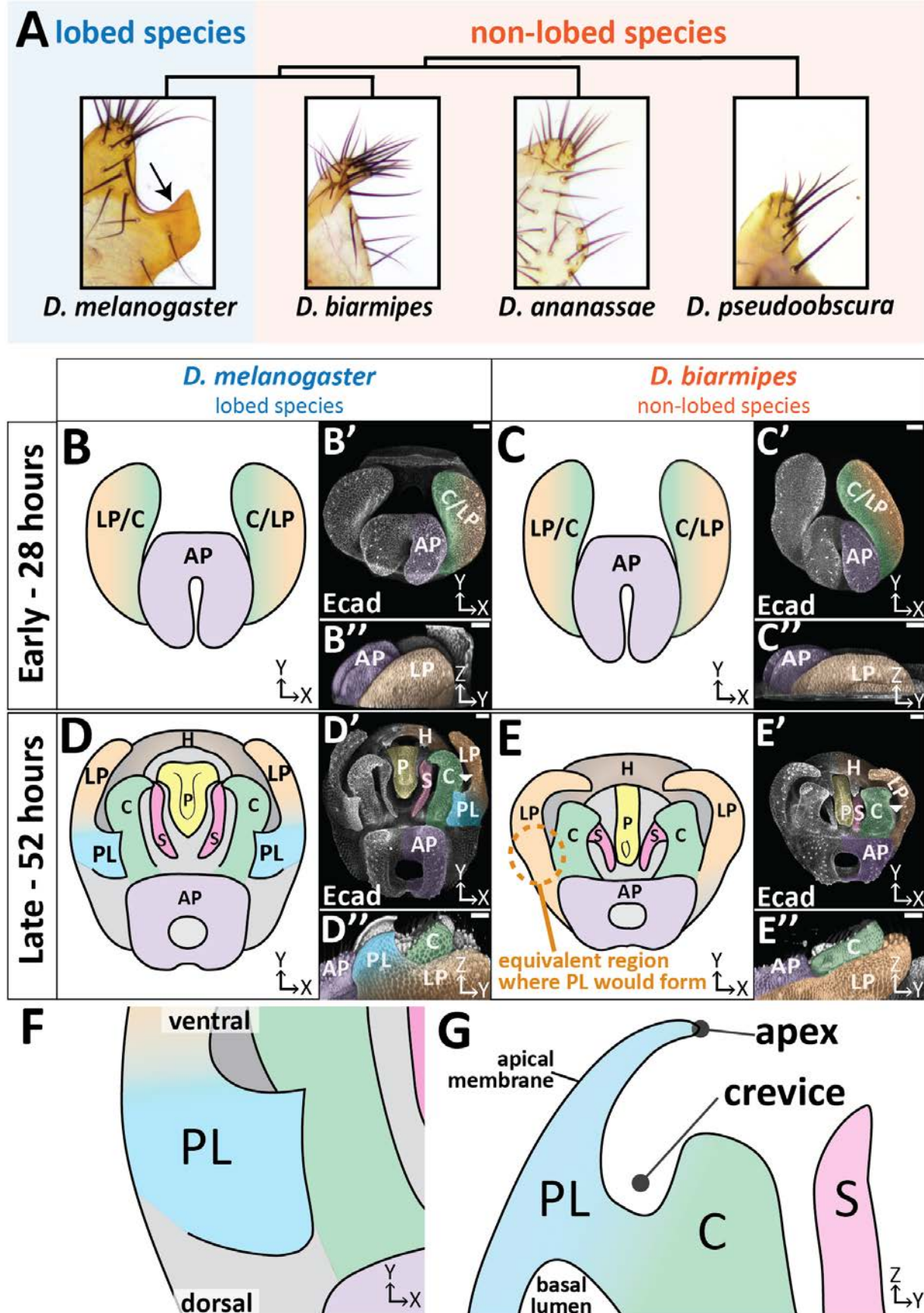
- 670 Lecuit, T., & Lenne, P.F. (2007). Cell surface mechanics and the control of cell shape, tissue
671 patterns and morphogenesis. *Nature Reviews. Molecular Cell Biology*, 8(8), 633–644.
672 <https://doi.org/10.1038/nrm2222>
- 673 LeVasseur-Viens, H., Polak, M., & Moehring, A.J. (2015). No evidence for external genital
674 morphology affecting cryptic female choice and reproductive isolation in *Drosophila*.
675 *Evolution*, 69(7), 1797–1807. <https://doi.org/10.1111/evo.12685>
- 676 Linde-Medina, M., & Marcucio, R. (2018). Living tissues are more than cell clusters: The
677 extracellular matrix as a driving force in morphogenesis. *Progress in Biophysics and*
678 *Molecular Biology*, 137, 46–51. <https://doi.org/10.1016/j.pbiomolbio.2018.01.009>
- 679 Li, L., Tang, Q., Nakamura, T., Suh, J.G., Ohshima, H., & Jung, H.S. (2016). Fine tuning of
680 Rac1 and RhoA alters cuspal shapes by remodeling the cellular geometry. *Scientific Reports*,
681 6, 37828. <https://doi.org/10.1038/srep37828>
- 682 Liu, Y., Ramos-Womack, M., Han, C., Reilly, P., Brackett, K.L., Rogers, W., Williams, T.M.,
683 Andolfatto, P., Stern, D.L. and Rebeiz, M. (2019). Changes throughout a Genetic network
684 mask the contribution of hox gene evolution. *Current Biology* 29, 1-10.
685 <https://doi.org/10.1016/j.cub.2019.05.074>
- 686 Loganathan, R., Rongish, B.J., Smith, C.M., Filla, M.B., Czirok, A., Bénazéraf, B., & Little, C.D.
687 (2016). Extracellular matrix motion and early morphogenesis. *Development*, 143(12), 2056–
688 2065. <https://doi.org/10.1242/dev.127886>
- 689 Mancuso, V.P., Parry, J.M., Storer, L., Poggioli, C., Nguyen, K.C.Q., Hall, D.H., & Sundaram,
690 M.V. (2012). Extracellular leucine-rich repeat proteins are required to organize the apical
691 extracellular matrix and maintain epithelial junction integrity in *C. elegans*. *Development*,
692 139(5), 979–990. <https://doi.org/10.1242/dev.075135>
- 693 Martin, A.C., & Goldstein, B. (2014). Apical constriction: themes and variations on a cellular
694 mechanism driving morphogenesis. *Development*, 141(10), 1987–1998.
695 <https://doi.org/10.1242/dev.102228>
- 696 Moczek, A.P. (2008). On the origins of novelty in development and evolution. *BioEssays*, 30(5),
697 432–447. <https://doi.org/10.1002/bies.20754>
- 698 Osterfield, M., Schüpbach, T., Wieschaus, E., & Shvartsman, S.Y. (2015). Diversity of epithelial
699 morphogenesis during eggshell formation in drosophilids. *Development*, 142(11), 1971–
700 1977. <https://doi.org/10.1242/dev.119404>
- 701 Paluch, E., & Heisenberg, C.P. (2009). Biology and physics of cell shape changes in
702 development. *Current Biology*, 19(17), R790-799. <https://doi.org/10.1016/j.cub.2009.07.029>

- 703 Peter, I.S., & Davidson, E.H. (2015). *Genomic Control Process: Development and Evolution*.
704 Academic Press.
- 705 Ray, R.P., Matamoro-Vidal, A., Ribeiro, P.S., Tapon, N., Houle, D., Salazar-Ciudad, I., &
706 Thompson, B.J. (2015). Patterned anchorage to the apical extracellular matrix defines tissue
707 shape in the developing appendages of drosophila. *Developmental Cell*, 34(3), 310–322.
708 <https://doi.org/10.1016/j.devcel.2015.06.019>
- 709 Rebeiz, M., Patel, N.H., & Hinman, V.F. (2015). Unraveling the tangled skein: the evolution of
710 transcriptional regulatory networks in development. *Annual Review of Genomics and Human*
711 *Genetics*, 16, 103–131. <https://doi.org/10.1146/annurev-genom-091212-153423>
- 712 Rebeiz, M., Pool, J.E., Kassner, V.A., Aquadro, C.F., & Carroll, S.B. (2009). Stepwise
713 modification of a modular enhancer underlies adaptation in a Drosophila population.
714 *Science*, 326(5960), 1663–1667. <https://doi.org/10.1126/science.1178357>
- 715 Rebeiz, M., & Posakony, J.W. (2004). GenePalette: a universal software tool for genome
716 sequence visualization and analysis. *Developmental Biology*, 271(2), 431–438.
717 <https://doi.org/10.1016/j.ydbio.2004.04.011>
- 718 Renvoisé, E., Kavanagh, K.D., Lazzari, V., Häkkinen, T.J., Rice, R., Pantalacci, S., Salazar-
719 Ciudad, I., Jernvall, J. (2017). Mechanical constraint from growing jaw facilitates mammalian
720 dental diversity. *Proceedings of the National Academy of Sciences of the United States of*
721 *America*, 114(35), 9403–9408. <https://doi.org/10.1073/pnas.1707410114>
- 722 Rice, G., David, J., Kamimura, Y., Masly, J., Mcgregor, A., Nagy, O., Noselli, S., Nunes, M.D.S.,
723 O'Grady, P., Sánchez-Herrero, E., Siegal, M., Toda, M., Rebeiz, M., Courtier-Orgogozo, V.,
724 & Yassin, A. (2019). A Standardized Nomenclature and Atlas of the Male Terminalia of
725 *Drosophila melanogaster*. *Preprints*, 2019060071.
726 <https://doi.org/10.20944/preprints201906.0071.v1>
- 727 Roll-Mecak, A. (2019). How cells exploit tubulin diversity to build functional cellular microtubule
728 mosaics. *Current Opinion in Cell Biology*, 56, 102–108.
729 <https://doi.org/10.1016/j.ceb.2018.10.009>
- 730 Schindelin, J., Arganda-Carreras, I., Frise, E., Kaynig, V., Longair, M., Pietzsch, T., Preibisch,
731 S., Rueden, C., Saalfeld, S., Schmid, B., Tinevez, J.Y., White, D.J., Hartenstein, V., Eliceiri,
732 K., Tomancak, P., Cardona, A. (2012). Fiji: an open-source platform for biological-image
733 analysis. *Nature Methods*, 9(7), 676–682. <https://doi.org/10.1038/nmeth.2019>
- 734 Schnatwinkel, C., & Niswander, L. (2013). Multiparametric image analysis of lung-branching
735 morphogenesis. *Developmental Dynamics*, 242(6), 622–637.
736 <https://doi.org/10.1002/dvdy.23961>

- 737 Smith, S.J., Rebeiz, M., & Davidson, L. (2018). From pattern to process: studies at the interface
738 of gene regulatory networks, morphogenesis, and evolution. *Current Opinion in Genetics &*
739 *Development*, 51, 103–110. <https://doi.org/10.1016/j.gde.2018.08.004>
- 740 Smith, A.F., Posakony, J.W., & Rebeiz, M. (2017). Automated tools for comparative sequence
741 analysis of genic regions using the GenePalette application. *Developmental Biology*, 429(1),
742 158-164. <https://doi.org/10.1016/j.ydbio.2017.06.033>
- 743 Tada, M., & Heisenberg, C.P. (2012). Convergent extension: using collective cell migration and
744 cell intercalation to shape embryos. *Development*, 139(21), 3897–3904.
745 <https://doi.org/10.1242/dev.073007>
- 746 Tanaka, K., Barmina, O., & Kopp, A. (2009). Distinct developmental mechanisms underlie the
747 evolutionary diversification of Drosophila sex combs. *Proceedings of the National Academy*
748 *of Sciences of the United States of America*, 106(12), 4764–4769.
749 <https://doi.org/10.1073/pnas.0807875106>
- 750 Tian, E., & Ten Hagen, K.G. (2007). O-linked glycan expression during Drosophila
751 development. *Glycobiology*, 17(8), 820–827. <https://doi.org/10.1093/glycob/cwm056>
- 752 Wagner, G.P. (2014). *Homology, Genes, and Evolutionary Innovation*. Princeton, NJ: Princeton
753 University Press.
- 754 Wagner, G.P. & Lynch, V.J. (2010). Evolutionary novelties. *Current Biology*, 20(2), R48-52.
755 <https://doi.org/10.1016/j.cub.2009.11.010>
- 756 Walck-Shannon, E., & Hardin, J. (2014). Cell intercalation from top to bottom. *Nature Reviews.*
757 *Molecular Cell Biology*, 15(1), 34–48. <https://doi.org/10.1038/nrm3723>
- 758 Wang, X., Harris, R. E., Bayston, L. J., & Ashe, H. L. (2008). Type IV collagens regulate BMP
759 signalling in Drosophila. *Nature*, 455(7209), 72–77. <https://doi.org/10.1038/nature07214>
- 760 Webster, D.R., Gundersen, G.G., Bulinski, J.C., & Borisy, G.G. (1987). Differential turnover of
761 tyrosinated and detyrosinated microtubules. *Proceedings of the National Academy of*
762 *Sciences of the United States of America*, 84(24), 9040–9044.
763 <https://doi.org/10.1073/pnas.84.24.9040>
- 764 Wilkin, M. B., Becker, M. N., Mulvey, D., Phan, I., Chao, A., Cooper, K., Chung H.J., Campbell,
765 I.D., Baron, M., MacIntyre, R. (2000). Drosophila dumpy is a gigantic extracellular protein
766 required to maintain tension at epidermal-cuticle attachment sites. *Current Biology*, 10(10),
767 559–567. [https://doi.org/10.1016/S0960-9822\(00\)00482-6](https://doi.org/10.1016/S0960-9822(00)00482-6)
- 768 Xu, Z., Schaedel, L., Portran, D., Aguilar, A., Gaillard, J., Marinkovich, M.P. Théry, M., &
769 Nachury, M.V. (2017). Microtubules acquire resistance from mechanical breakage through
770 intraluminal acetylation. *Science*, 356(6335), 328–332.

771 <https://doi.org/10.1126/science.aai8764>

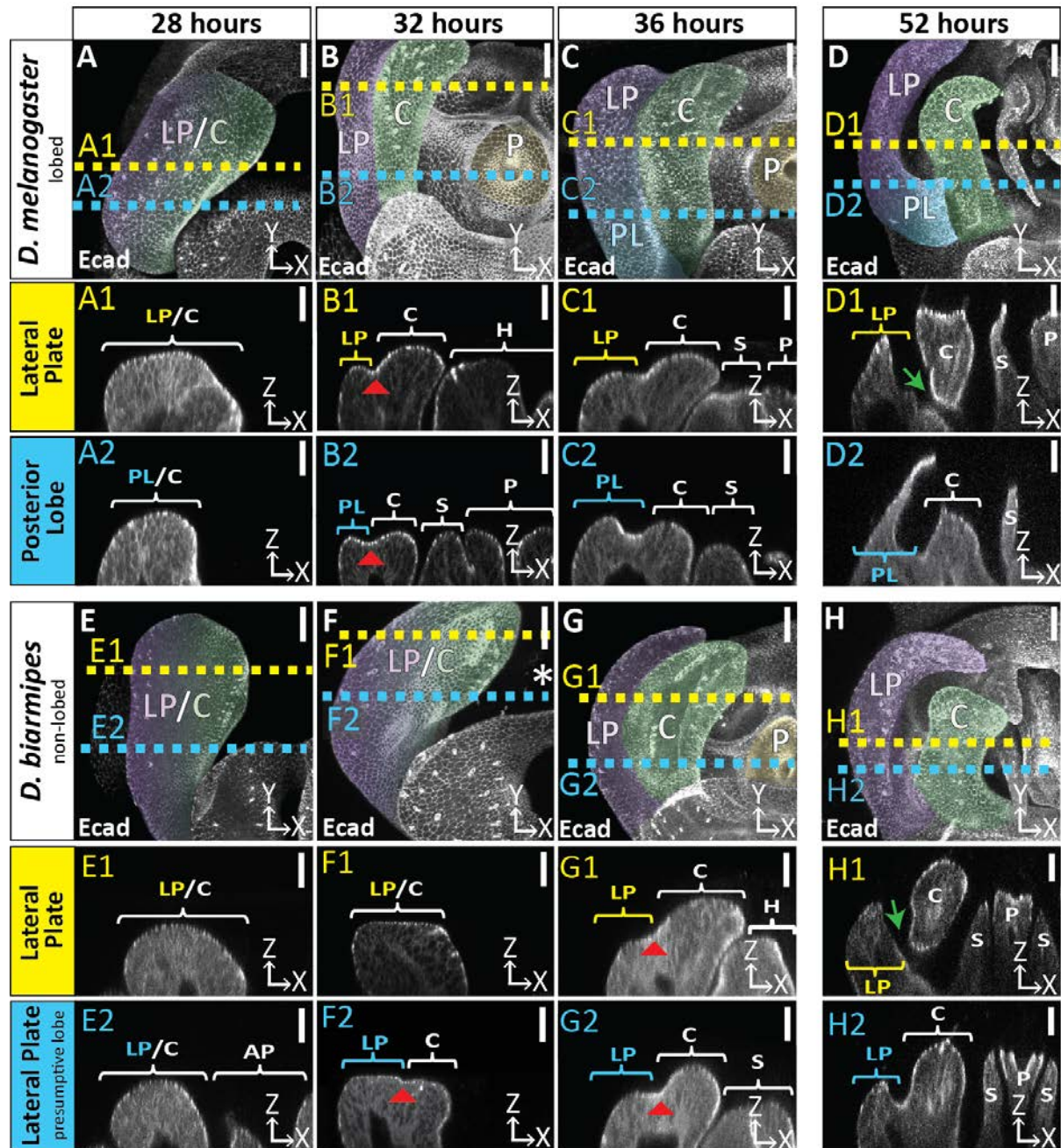
772 Figure 1



773 **Figure 1. The posterior lobe protrudes from the lateral plate.**

774 (A) Phylogenetic tree with representative bright-field images of adult cuticle of the lateral plate
775 and posterior lobe (arrow). (B-E) Illustration, (B'-E') max projection, and (B''-E'') three-
776 dimensional projection of early (28 hours APF) and late (52 hours APF) developing genitalia
777 showing the posterior lobe projecting form the lateral plate of *D. melanogaster* (D''), but absent
778 in *D. biarmipes* (E''). Relevant structures are labeled: posterior lobe (PL), lateral plate (LP),
779 clasper (C), sheath (S), phallus (P), anal plate (AP), and hypandrium (H). (F) Zoomed in
780 illustration of posterior lobe and (G) a cross-sectional/lateral view of the posterior lobe.
781 Important terms are labeled. All max projections are oriented with ventral side towards to top
782 and dorsal sides towards the bottom. The highest point of the lobe is the apex and the
783 invagination between the lobe and the clasper is termed the crevice (G). Scale bar, 20µm.

784 Figure 1 – supplement 1



786 **Supplement 1 - figure 1 . Developmental timing of lobed vs non-lobed genitalia.**

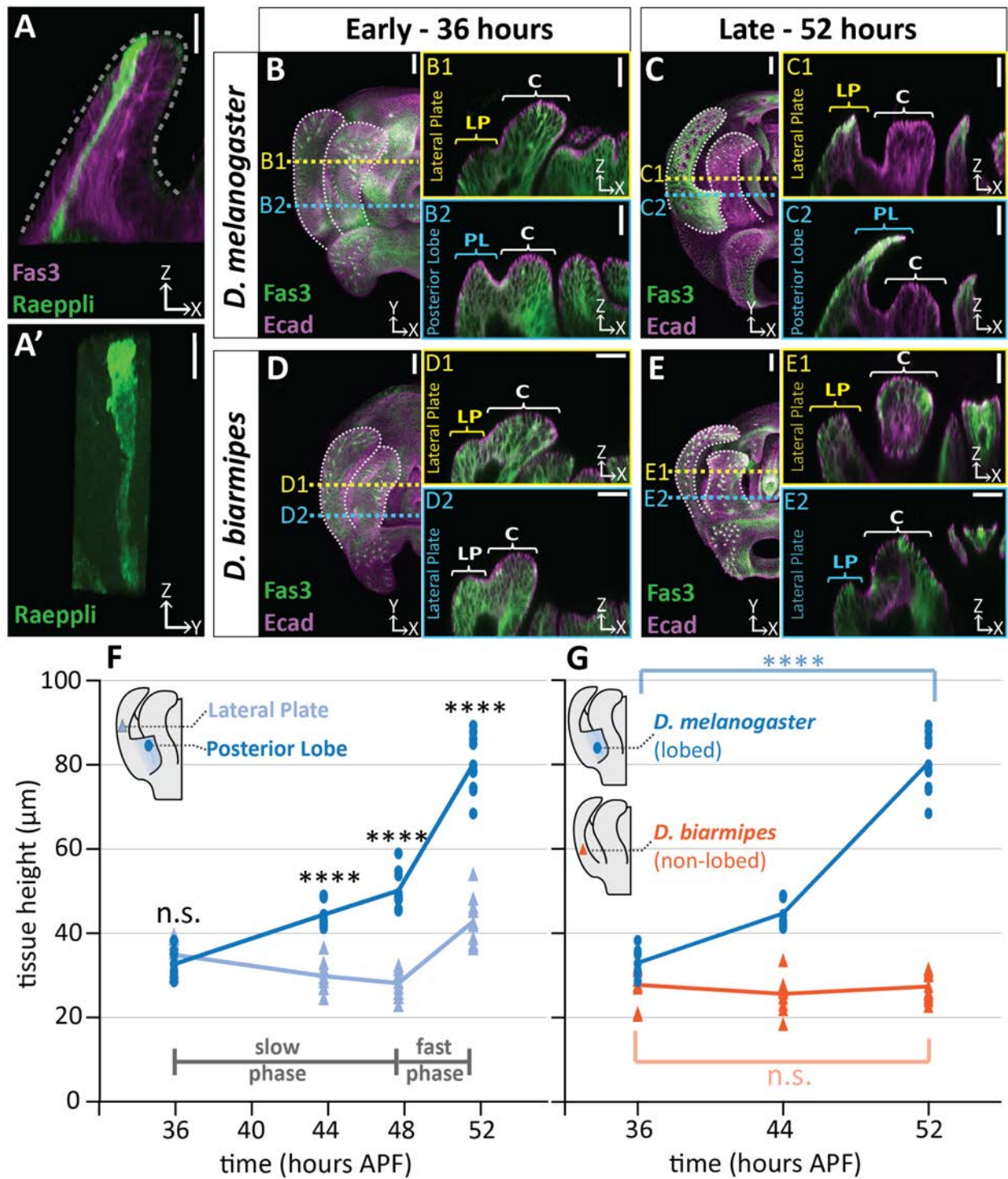
787 Developmental time course of the lobed species *D. melanogaster* (A-D) and the non-lobed
788 species *D. biarmipes* with E-cadherin label. Location of respective cross sections indicated in
789 yellow for lateral plate and blue for posterior lobe (*D. melanogaster*) or equivalent location in
790 non-lobed species (*D. biarmipes*). Relevant structures are labeled: posterior lobe (PL), lateral
791 plate (LP), clasper (C), sheath (S), and phallus (P). Scale bar, 20µm. At 28 hours APF the
792 genitalia looks relatively similar between *D. melanogaster* (A-A2) and *D. biarmipes* (E-E2). At 32
793 hours APF in *D. melanogaster* the clasper and lateral plate have fully begun to cleave (B1-2 red
794 arrowhead=cleavage), the lateral plate is lower than the clasper (B1), and the hypandrium,
795 sheath, and phallus have fully everted and are neighboring the clasper and lateral plate (B1-2).
796 *D. biarmipes* lags behind approximately 4 hours. At 32 hours APF there is slight cleavage near
797 the dorsal side of the lateral plate and clasper (F2 red arrowhead), but no cleavage has
798 occurred at the ventral side(F1). In addition, the sheath, hypandrium, and phallus have not
799 everted yet (F1-2). At 36 hours APF in *D. biarmipes* cleavage has begun along the full length of
800 the lateral plate and clasper (G1-2 red arrowhead), the lateral plate is lower than the clasper
801 (G1-2), and the hypandrium, sheath, and phallus have everted and are next to the lateral plate
802 and clasper (G1-2). As development proceeds later at 52 hours APF the lateral plate and
803 clasper fully separate at the ventral side of the genitalia in both *D. melanogaster* (D1 green
804 arrow) and *D. biarmipes* (H1 green arrow). Full cleavage does not span the length of the lateral
805 plate and clasper (D2 and H2) and stops right before the posterior lobe forms (D2) and also
806 stops before reaching the very dorsal side of the lateral plate and clasper in *D. biarmipes* (H2).

808 **Supplement 1 - video 1. The posterior lobe protrudes from the lateral plate.**

809 Three-dimensional projections of *D. melanogaster* (left) and *D. biarmipes* (right) samples at 52

810 hours APF labeled with E-cadherin.

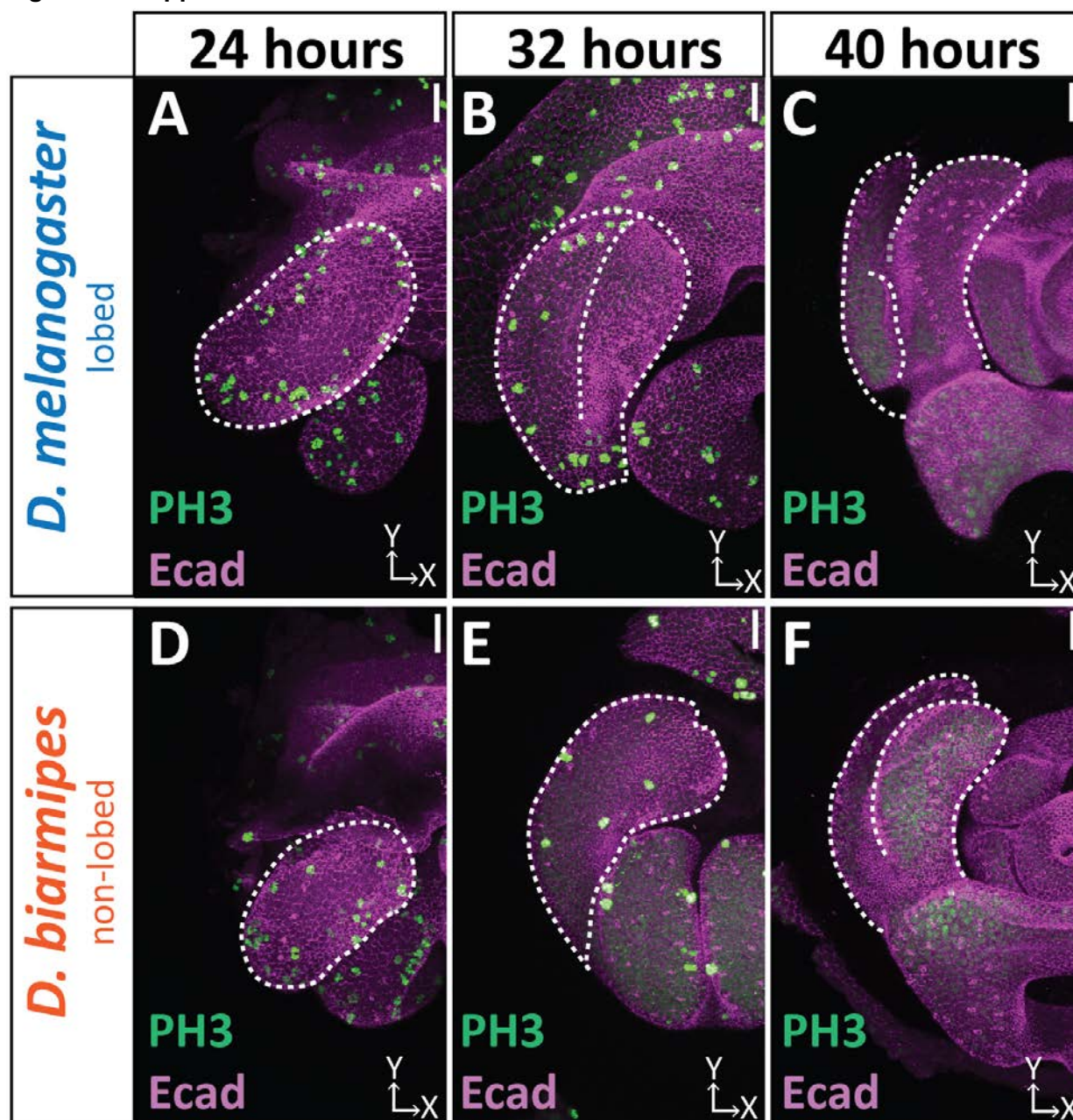
811 **Figure 2**



812 **Figure 2. Posterior lobe cells increase in height to project out from the lateral plate.**

813 (A) A single cell in the posterior lobe labeled with Raeppli-mTFP1 (green) spans the height of
814 the tissue labeled with lateral membrane marker fasciclin III (Fas3, magenta). Apical side of
815 posterior lobe identified with dotted line. Sample is 44h after pupal formation (APF), but was
816 heat shocked for 1 hour at 24h APF causing it to develop faster and more closely resembles a
817 48h APF sample. Scale bar, 10 μ m. n=4 (B-E) Maximum projections of early (36h APF) and late
818 (52h APF) genital samples labeled with Fas3 (lateral membranes, green) and E-Cadherin
819 (apical membranes, magenta). Location of respective cross sections indicated in yellow for
820 lateral plate (B1-E1) and blue for posterior lobe (*D. melanogaster*) or equivalent location in non-
821 lobed species (*D. biarmipes*) (B2-E2). Scale bar, 20 μ m. (F) Quantification of tissue thickness of
822 the lateral plate (light blue) and posterior lobe (dark blue). Illustration represents approximate
823 location of cross-section that was used for tissue height measurement. Individual data points a
824 presented; n=10 per each time point. (G) Quantification of tissue thickness of the posterior lobe
825 in *D. melanogaster* (dark blue) and equivalent location in non-lobed species *D. biarmipes*
826 (orange). Illustration represents approximate location of cross-section that was used for tissue
827 thickness measurement. Individual data points presented; n \geq 9 per each time point. Statistical
828 significance is indicated (unpaired t-test; ****p \leq 0.0001; n.s.=not significant p \geq 0.05). *D.*
829 *melanogaster* tissue height measures in (G) are replotted from (F) to facilitate direct
830 comparisons with *D. biarmipes*.

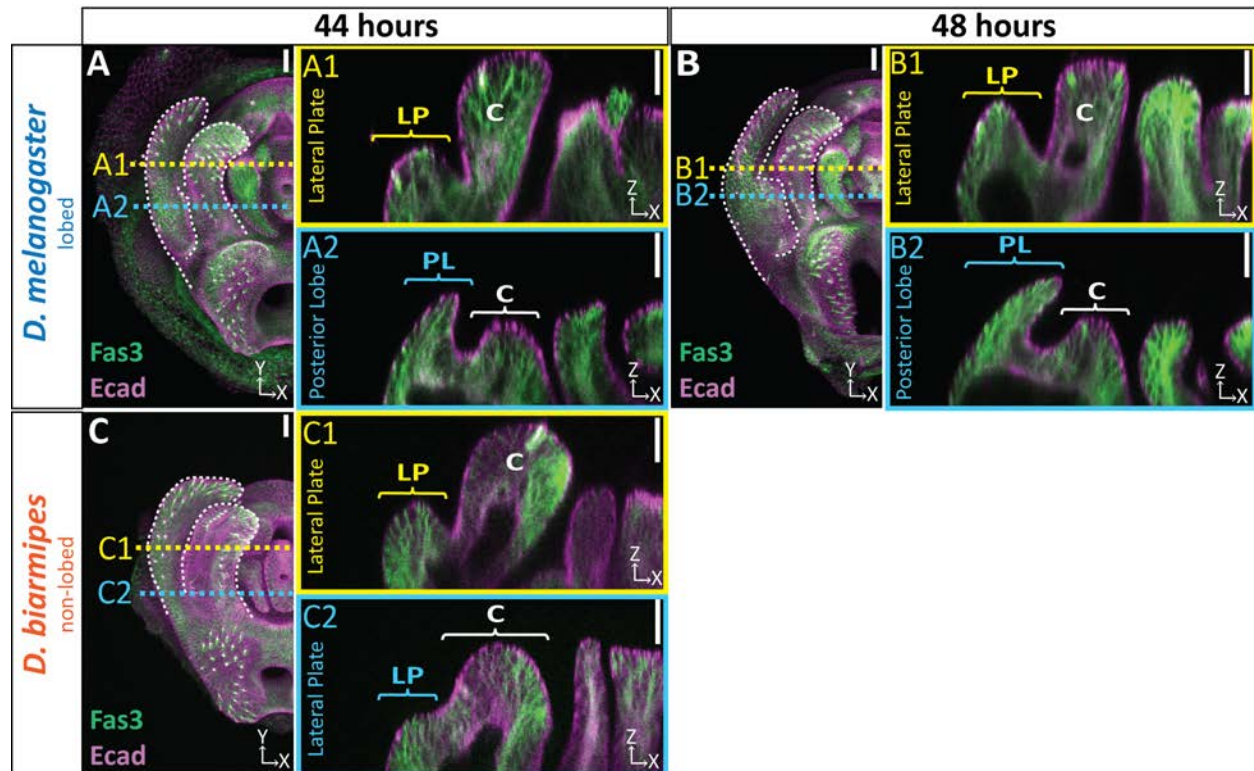
831 Figure 2 – supplement 1



832 **Figure 2 - supplement 1. Cell division dynamics do not differ between lobed and non-**
833 **lobed species.**

834 Developmental time course with Phospho-Histone H3 (Ser 10) (PH3; green) labeling actively dividing
835 cells and Ecad (magenta) labeling the apical membrane of the tissue. Only superficial slices are shown to
836 avoid fat body signals beneath lateral plate and clasper. $n \geq 3$ per each time point. Scale bar, 20 μ m. In
837 both *D. melanogaster* and *D. biarmipes* cell division is widespread at 24 hours APF (A & D). Cell division
838 is decreased by 32 hours APF (B & E). By 40 hours APF no cell division is occurring (C & F).

839 Figure 2 – supplement 2



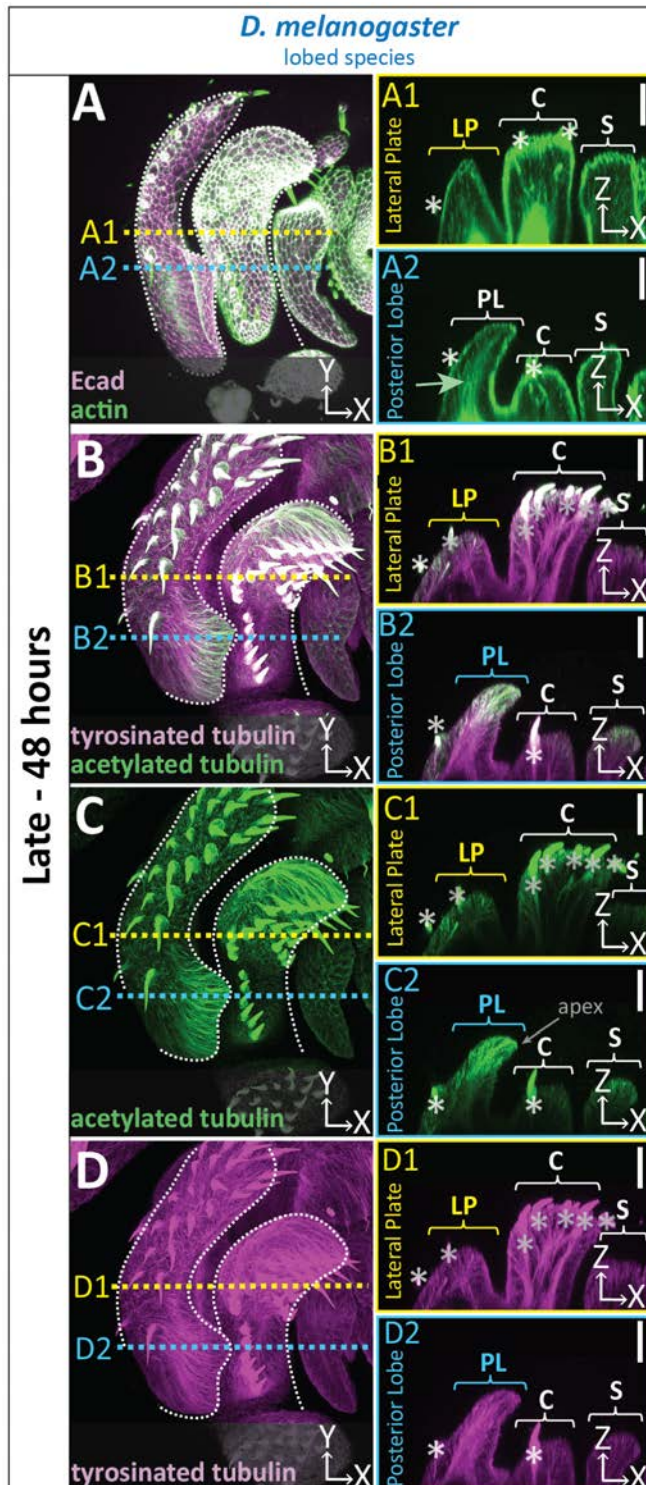
840 **Figure 2 - supplement 2. Extended time course for tissue thickness in lobed and non-**
841 **lobed species.**

842 Extended time course for samples quantified in Figure 2F-G. (A-C) Max and cross-section view of 44
843 hours APF (A & C) and 48 hours APF (B) genital samples with lateral membrane labeled with Fas3
844 (green) and apical membrane labeled with Ecad (magenta). Location of respective cross sections
845 indicated in yellow for lateral plate (A1-C1) and blue for posterior lobe (*D. melanogaster*) or equivalent
846 location in non-lobed species (*D. biarmipes*) (A2-C2). $n \geq 9$ per experiment. Scale bar, 20 μ m.

848 **Figure 2 - video 1. Cell rearrangement during posterior lobe development.**

849 Live imaging of posterior lobe development with GFP tagged armadillo (apical membrane
850 marker) illustrating a cell dropping from the apical surface and a neighboring cell filling in the
851 gap. Imaging starts at approximately 36 hours APF. Due to uncontrolled temperatures during
852 imaging that were cooler than normal growing conditions, the posterior lobe develops slower
853 and the time indicated is not comparable to other images in the manuscript which were all
854 grown under controlled settings. Based on the thickness of the posterior lobe at the end of the
855 movie the posterior lobe is between 48 to 52 hours APF. Cells were tracked manually and
856 indicated with colored dots. Some dots disappear towards the end of the movie as they become
857 difficult to track due to the signal from cells on the medial side of the posterior lobe.

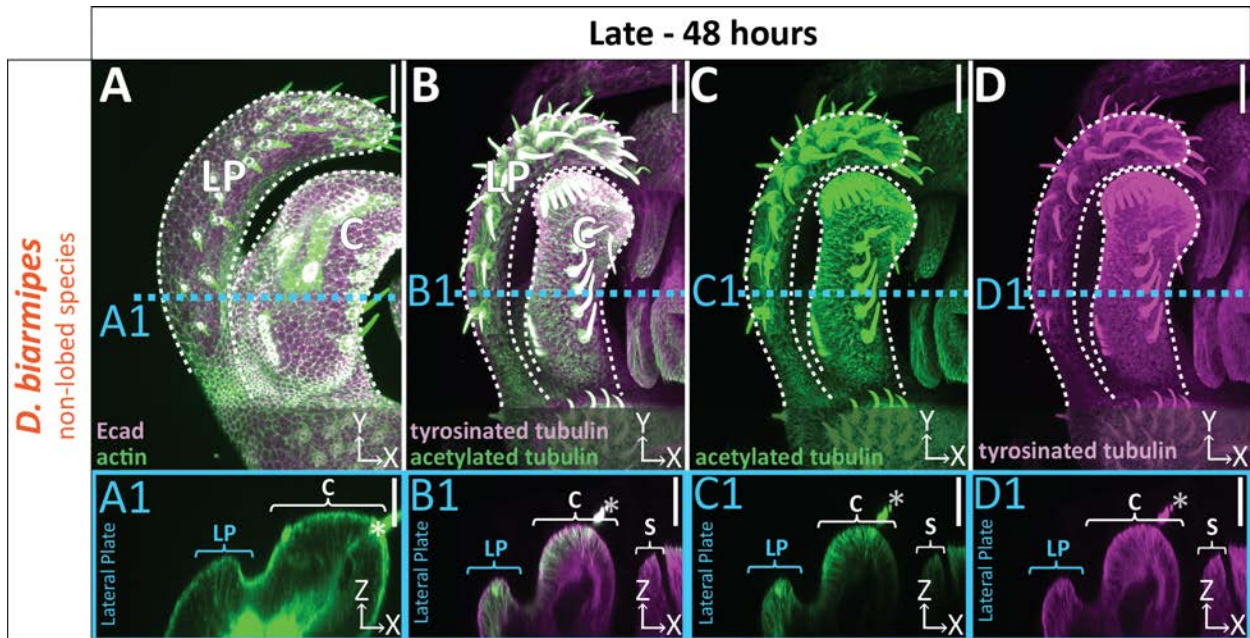
858 **Figure 3**



861 **Figure 3. Cytoskeletal components increased in posterior lobe cells.**

862 (A-D) Maximum projection, and respective cross-sections of late (48h APF) genital samples of
863 the lobed species *D. melanogaster* labeled with F-actin/phalloidin and Ecad (A), acetylated
864 tubulin (B,C), and tyrosinated tubulin (B,D). Location of respective cross sections indicated in
865 yellow for lateral plate (A1-D1) and blue for posterior lobe (A2-D2). Cross-sections are
866 maximum projections of a restricted 5.434 μ m thick section to provide a complete view of
867 cytoskeletal components along the apico-basal axis. All cross-sections are oriented with apical
868 side at the top and basal side at the bottom. Asterisk identifies bristles which have high levels of
869 F-actin and tubulin. Bright basal signal in A1 and A2 are fat bodies. Bottom layers were
870 removed in panel A to remove fat body signal which overwhelmed other details. (B-D2) Panels
871 C and D show separate channels of panel B. Relevant structures labeled: Posterior lobe (PL),
872 lateral plate (LP), clasper (C), and sheath (S). Scale bar, 20 μ m. n \geq 3 per experiment.

873 Figure 3 – supplement 1



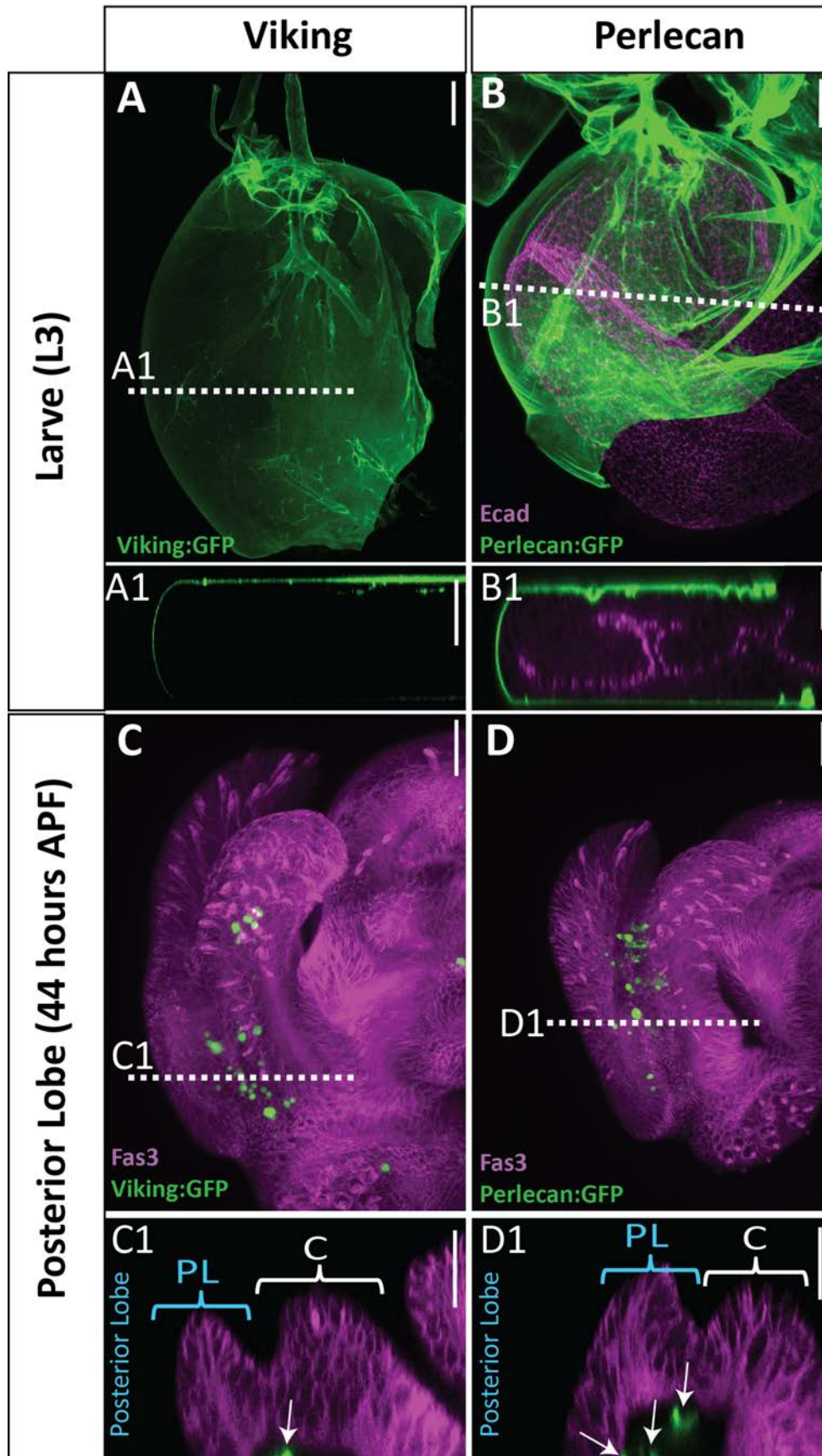
874 **Figure 3 - supplement 1. Uniform level of cytoskeletal components in non-lobed species.**

875 (A-D) Max projections of late (48h APF) genital samples of non-lobed species *D. biarmipes*
876 labeled with F-actin/phalloidin and Ecad (A), acetylated tubulin (B,C), and tyrosinated tubulin
877 (B,D). Location of respective cross sections indicated in blue for presumptive posterior lobe cells
878 (A1-D1). Cross-sections are maximum projection of a restricted 5.434 μ m thick section to display
879 the full view of the cytoskeleton along the apico-basal axis. All cross-sections are oriented with
880 apical side at the top and basal side at the bottom. Asterisk identifies bristles which have high
881 levels of F-actin and tubulin. Bright basal signal in A1 are fat bodies. Bottom layers were
882 removed in panel A to avoid fat body signal which masked other details. Panels C and D show
883 separate channels of panel B. Relevant structures labeled: Lateral plate (LP), clasper (C), and
884 sheath (S) labeled. Scale bar, 20 μ m. n \geq 3 per experiment.

886 **Figure 4. Dumpy deposition is correlated with posterior lobe development.**

887 (A-D) Max projection and (A'-B'') respective zoom, indicated with pink box, labeled with
888 Dumpy:YFP (green) and Ecad (magenta) for each time point. Location of respective cross
889 sections indicated in yellow for lateral plate (A1-D1) and blue for posterior lobe (A2-D2).
890 Arrowhead in (A2) indicates future posterior lobe cells. Cross-sections are oriented with apical
891 side at the top and basal side at the bottom. Relevant structures labeled: Posterior lobe (PL),
892 lateral plate (LP), clasper (C), sheath (S), and phallus (P). Scale bar, 20 μ m. n \geq 4 per
893 experiment. Images were independently brightened to show relevant structures.

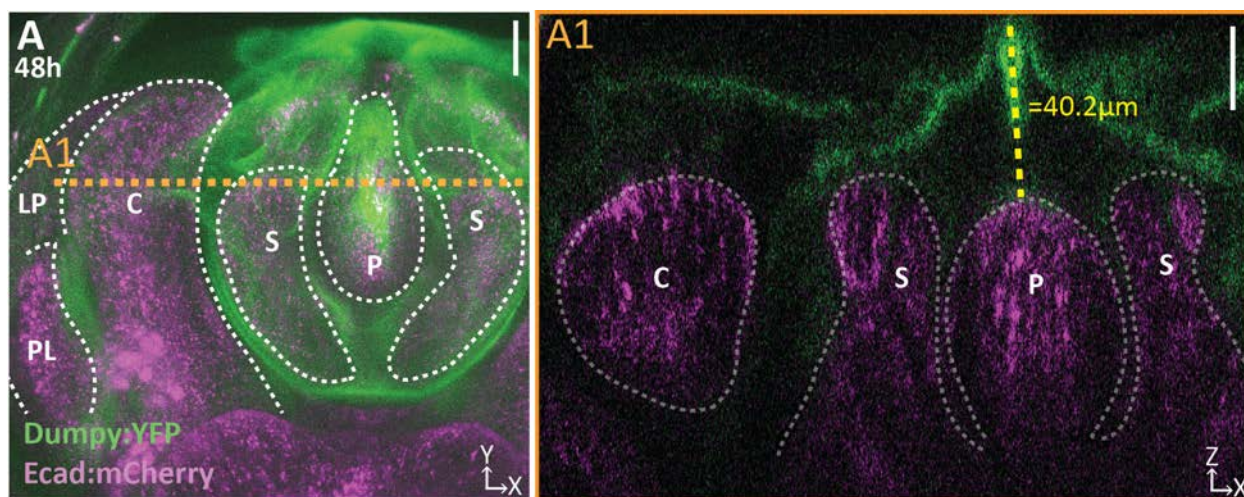
894 Figure 4 – supplement 1



896 **Figure 4 - supplement 1. Limited basal ECM present during posterior lobe**
897 **morphogenesis.**

898 Basal ECM markers Collagen IV (Viking:GFP; green)(A & C) and Perlecan (Perlecan:GFP;
899 green) (B & D) in L3 larval genital disc (A & B) and 44 hours APF genitalia (C & D). Image
900 settings were the same for each marker between larva and pupal samples. Sporadic dots
901 observed in genitalia fat bodies (arrow in cross section), which fill the basal lumen of the
902 genitalia. Location of respective cross sections indicated in white. Cross-sections for larval
903 samples are oriented basal sides out as the disc has not yet everted. Pupal samples are
904 oriented with apical side at the top and basal side at the bottom. Higher amounts of basal ECM
905 are observed in larval ECM compared to 44 hour APF genital samples. Relevant structures
906 labeled: Posterior lobe (PL) and clasper (C). Scale bar, 20µm.

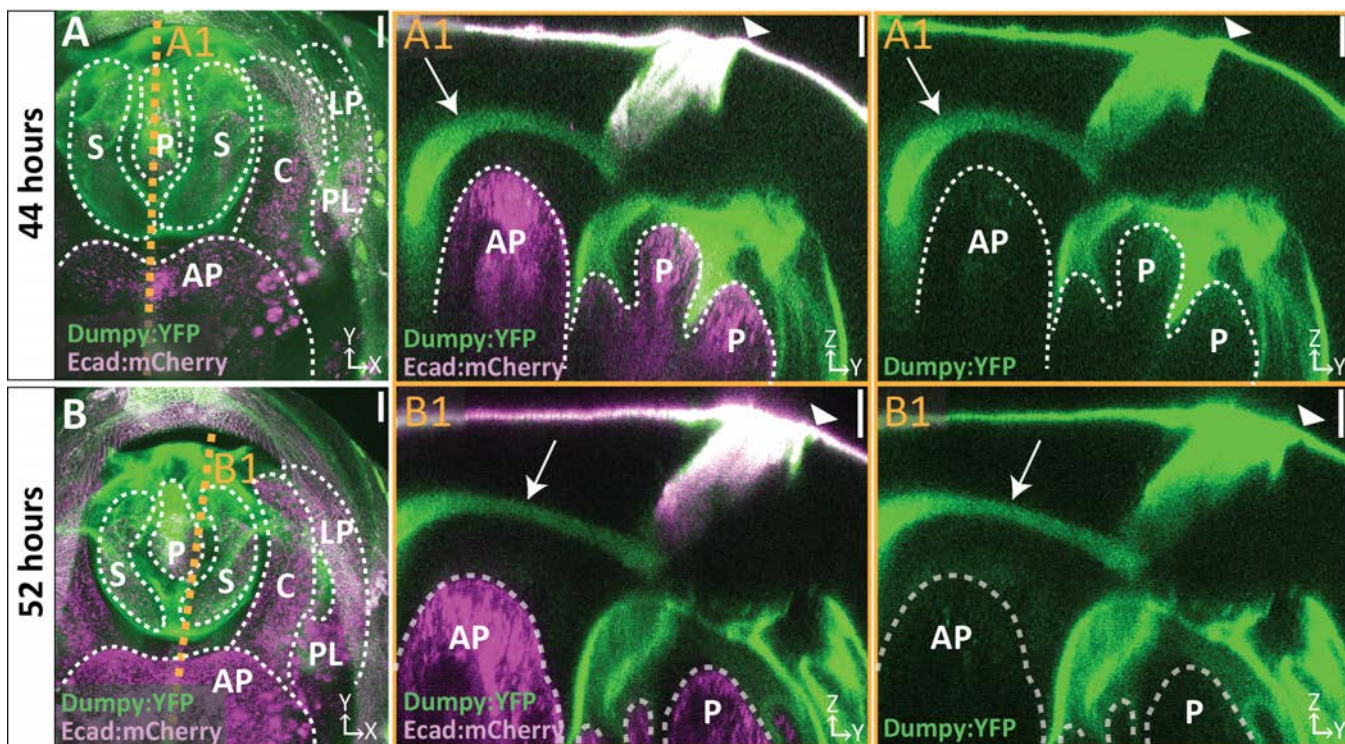
907 **Figure 4 – supplement 2**



908 **Figure 4 - supplement 2. Dumpy extends above the apical surface of the phallus.**

909 (A) Projection of Dumpy:YFP (green) and Ecad:mcherry (magenta) imaged live at 48 hours
910 APF. Location of respective cross sections indicated in orange. (A1) Cross section showing
911 extent of Dumpy:YFP observed above the surface of the genitalia. Relevant structures labeled:
912 Posterior lobe (PL), lateral plate (LP), clasper (C), sheath (S), and phallus (P). Scale bar, 20 μ m.
913 n=3.

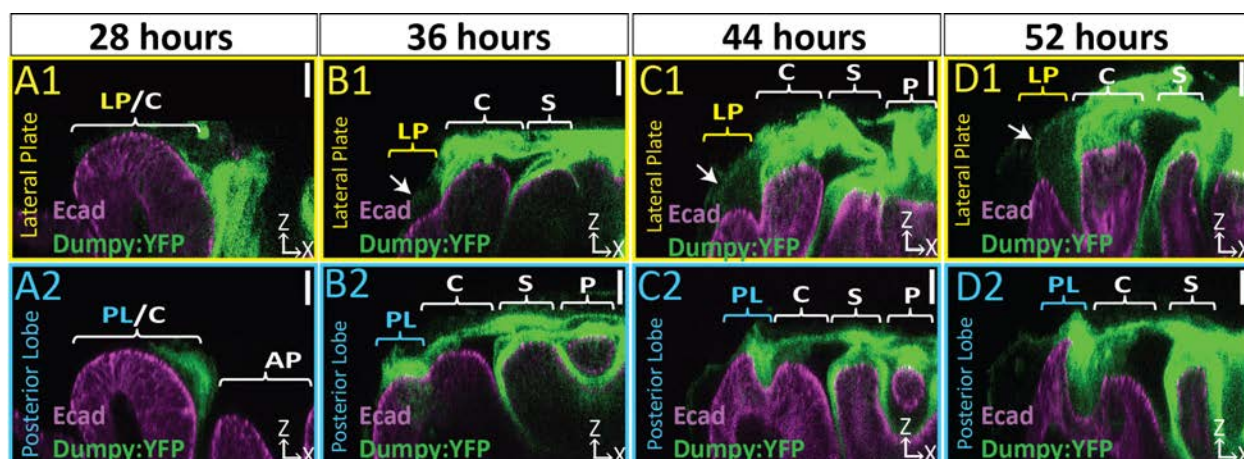
914 **Figure 4 – supplement 3**



915 **Figure 4 - supplement 3. A tether of Dumpy connects the genitalia to the pupal cuticle**
916 **membrane that encases the developing pupa.**

917 (A-B) Live imaging of Dumpy:YFP (green) and Ecad:mCherry (magenta) at respective time
918 points. Location of respective cross sections indicated in orange. (A1-B1) Cross-sections are
919 max projection of a 4.94 μ m (A1) and 1.73 μ m (B1) thick to show full tether (arrow) and its
920 connection to the cuticle (arrowhead) and anal plate. All cross-sections are oriented with apical
921 side at the top and basal side at the bottom. Relevant structures labeled: Posterior lobe (PL),
922 lateral plate (LP), clasper (C), sheath (S), phallus (P), and anal plate (AP). Scale bar, 20 μ m. n=1
923 per each time point.

924 Figure 4 – supplement 4



925 **Figure 4 - supplement 4. Weak aECM connection to lateral plate.**

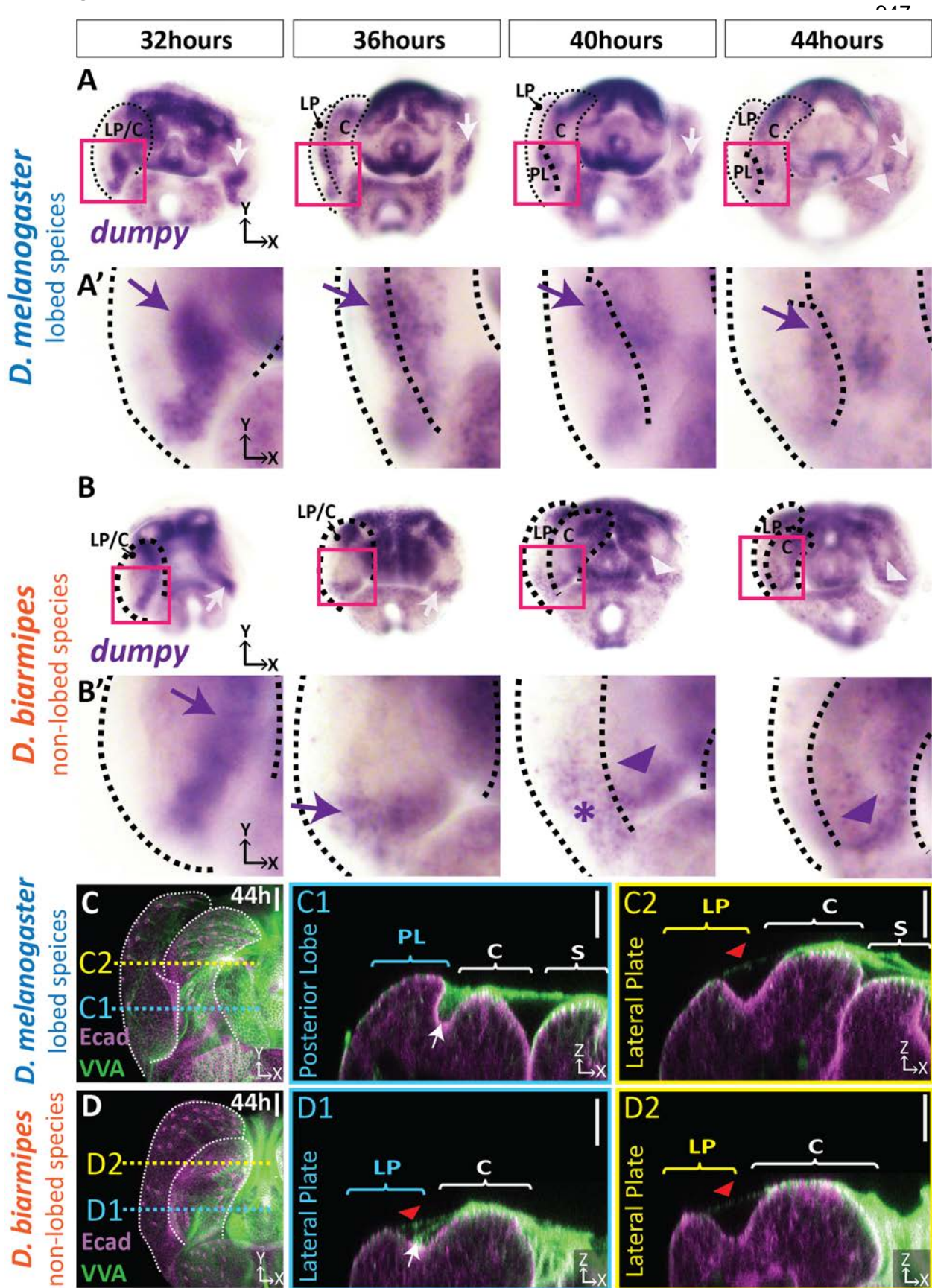
926 (A-D) Respective cross sections from Figure 2 of lateral plate (A1-D1) in yellow and posterior
927 lobe in blue (A2-D2). Cross-sections are oriented with apical side at the top and basal side at
928 the bottom. Relevant structure labeled: Posterior lobe (PL), lateral plate (LP), clasper (C),
929 sheath (S), and phallus (P). Scale bar, 20 μ m. n \geq 4 per experiment. Images were overexposed
930 to show relevant structures.

932 **Figure 4 - video 1. Three-dimensional structure of Dumpy on developing genitalia.**

933 Part 1 of the movie shows 3D rotation of 52 hour APF genital sample with Dumpy:YFP (green)
934 and E-cadherin (magenta) labels. Part 2 of the movie show a cross-sectional view starting at the
935 ventral side of the posterior lobe and moving towards the dorsal side of the posterior lobe and
936 part 3 shows the same view but starting at the ventral tip of the lateral plate and moving towards
937 the ventral side of the posterior lobe. In the upper-right corner there is a guide that roughly
938 depicts where the cross section is located. Cross-sections are oriented with apical side at the
939 top and basal side at the bottom. Relevant structures labeled: Posterior lobe (PL), lateral plate
940 (LP), clasper (C), sheath (S), and phallus (P).

942 **Figure 4 – video 2. A tether of Dumpy connects the genitalia to the surrounding cuticle.**
943 3D rotation of Dumpy:YFP (green) and Ecad:mCherry (magenta) imaged live at 44 hours APF.
944 Relevant structures labeled: Posterior lobe (PL), lateral plate (LP), clasper (C), sheath (S),
945 phallus (P), and anal plate (AP).

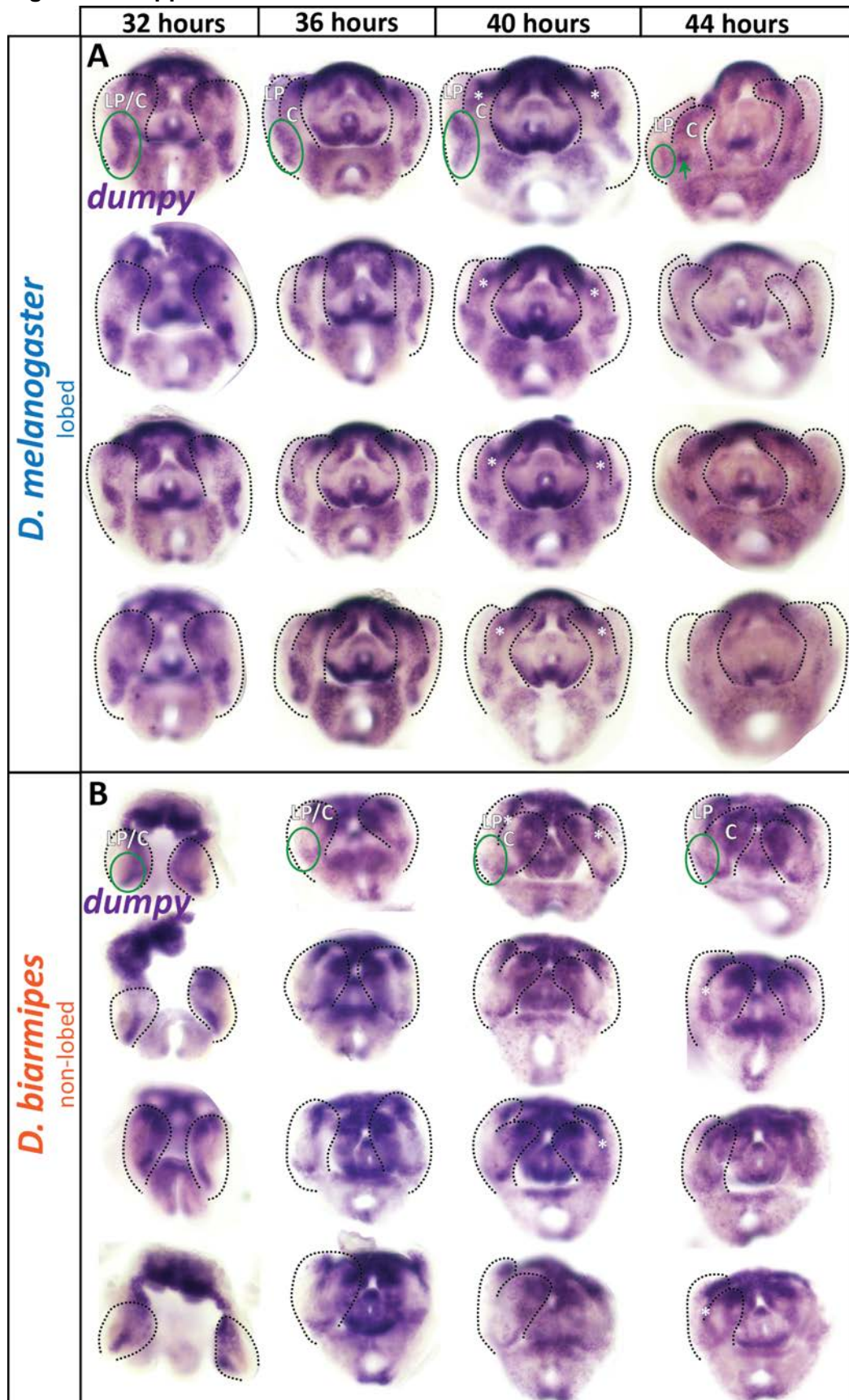
946 **Figure 5**



952 **Figure 5. aECM spatially expanded in lobed species compared to non-lobed species.**

953 (A-B) *in situ* hybridization for *dumpy* mRNA in lobed species *D. melanogaster* (A) and non-lobed
954 species *D. biarmipes* (B). Pink box outlines location of zoom in for A1 and B1. Relevant
955 expression highlighted with arrow (purple/white) for strong expression, asterisk for weak
956 expression, and arrowhead for clasper specific expression. (C-D) aECM is labeled with *Vicia*
957 *villosa* lectin (VVA; green) and apical membrane labeled with Ecad (magenta) at 44 hours APF
958 in *D. melanogaster* (C) and *D. biarmipes* (D). Location of respective cross sections indicated in
959 yellow for lateral plate (C1-D1) and blue for posterior lobe in *D. melanogaster* (C2) and
960 presumptive lobe cells in *D. biarmipes* (D2). All cross-sections are oriented with apical side at
961 the top and basal side at the bottom. White arrows highlight the crevice localization between the
962 lateral plate and clasper, which the aECM fills in *D. melanogaster* (C2), but only a weakly
963 stained strand-like structure of aECM appears in *D. biarmipes* (D2). Tendrils of aECM can also
964 be observed connecting to the lateral plate in both species (red arrowheads). Relevant
965 structures labeled: Posterior lobe (PL), lateral plate (LP), clasper (C), sheath (S), and phallus
966 (P). Scale bar, 20 μ m. n=at least 5 per experiment.

967 Figure 5 – supplement 1

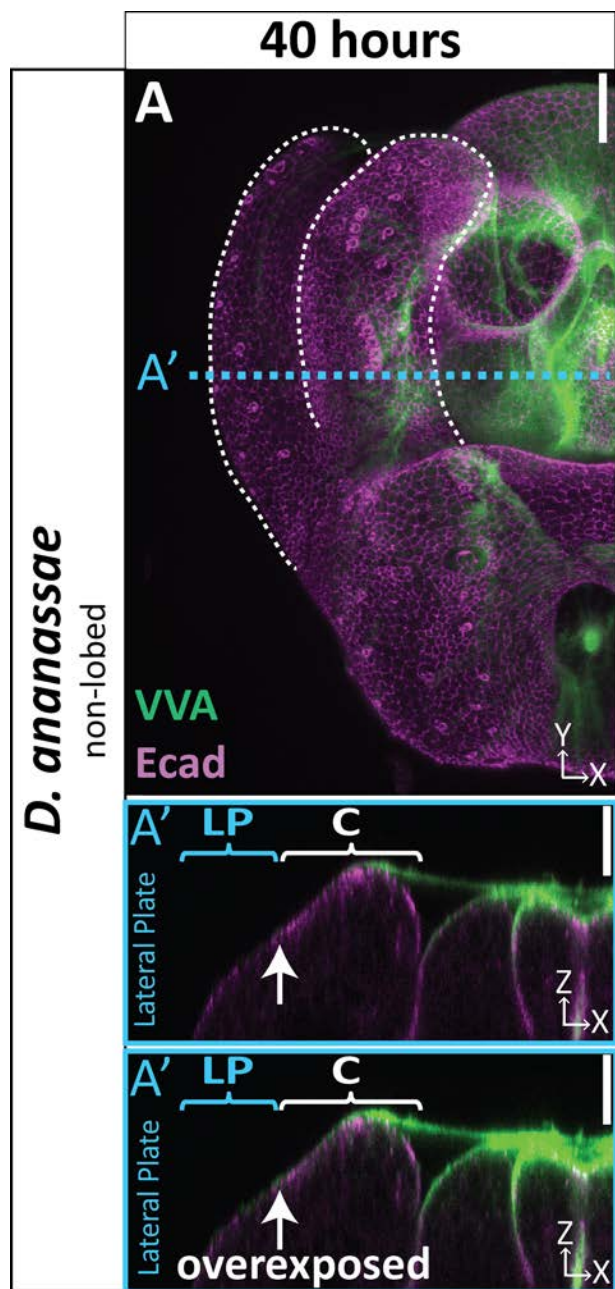


970 **Figure 5 - supplement 1. aECM spatially expanded in lobed species compared to non-**
971 **lobed species.**

972 (A-B) additional *in situ* hybridization samples for *dumpy* mRNA in lobed species *D.*
973 *melanogaster* (A) and non-lobed species *D. biarmipes* (B) to show full range of expression
974 observed in experiment. Outlines are approximations as details of structures are not easily
975 visible. Samples without outlines on one side are due to the tissue being damaged on that side.
976 Green circle in first image highlights relevant location at the base of the lateral plate, but not
977 included in the remaining images to leave image unobstructed. Asterisk indicates the
978 expression is deep in the sample and not expressed in lateral plate or clasper cells. n= 4 per
979 experiment.

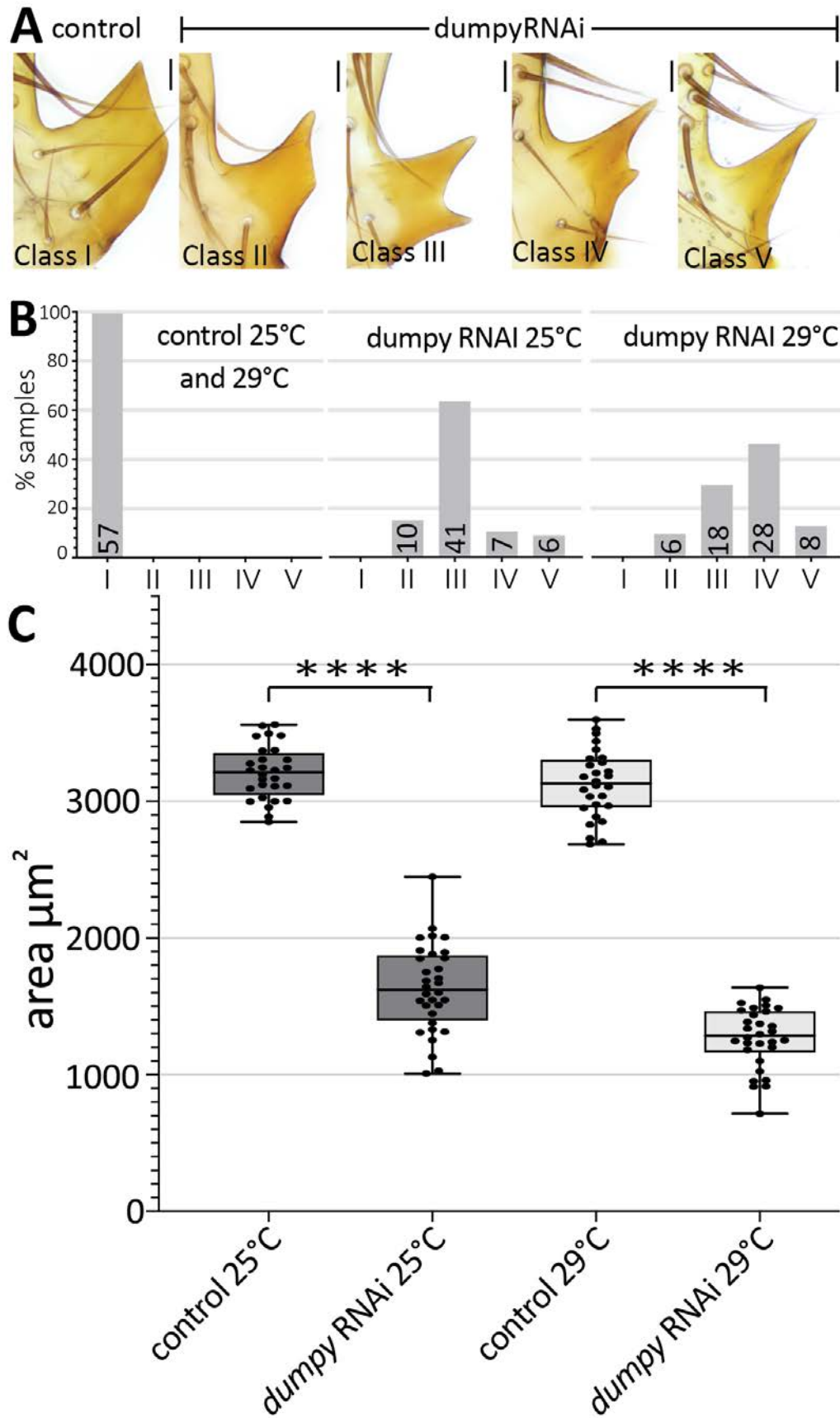
980

981 Figure 5 – supplement 2



982 **Figure 5 - supplement 2. aECM not expanded in non-lobed species *D. ananassae***
983 (A-C) aECM labeled with VVA (green) and apical membrane labeled with Ecad (magenta) at 40
984 hours APF in non-lobed species *D. ananassae*. Location of respective cross-sections indicated
985 in blue. Top cross-section displayed with normal brightness to show details and bottom cross-
986 section has been overexposed to show where all populations of aECM are located. All cross-
987 sections are oriented with apical side at the top and basal side at the bottom. White arrow
988 highlights the 'crevice' between the lateral plate and clasper, which is not pronounced at 40
989 hours APF in *D. ananassae*. Lateral plate (LP) and clasper (C) labeled in cross-section. Scale
990 bar, 20 μ m. n=at least 2 per experiment.

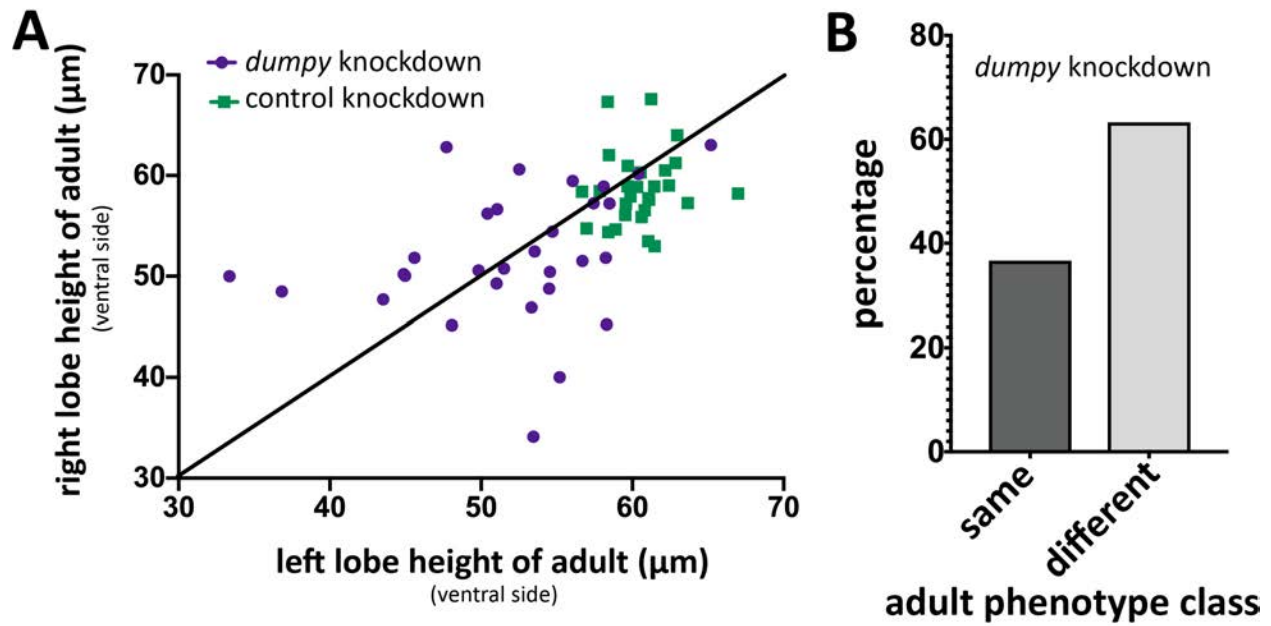
991 **Figure 6**



994 **Figure 6. Dumpy is required for proper posterior lobe shape.**

995 (A) Range of adult posterior lobe phenotypes produced by control (*mCherry* RNAi) and *dumpy*
996 RNAi animals. Phenotypic classes defined from wild type (I) to most severe (V). Scale bar,
997 20 μ m. (B) Percentage of posterior lobes in each class for control, *dumpy* RNAi at 25°C, and
998 *dumpy* RNAi at 29°C. (C) Quantification of area of adult posterior lobes of *mCherry* RNAi
999 (control) and *dumpy* RNAi at 25°C and 29 °C. Statistical significance between each temperature
1000 indicated (unpaired t-test; ****p \leq 0.0001).

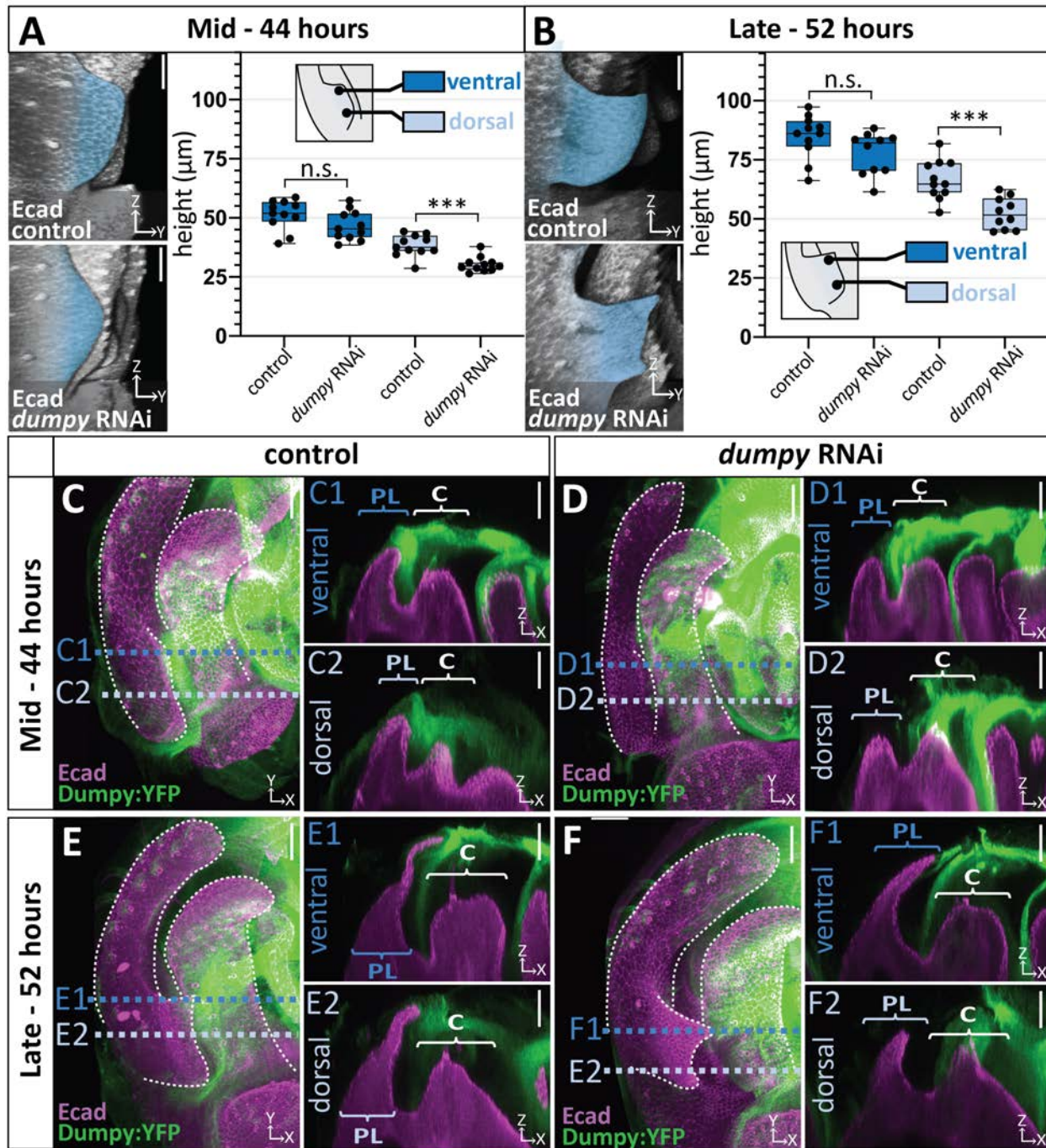
1001 **Figure 6 – supplement**



1002 **Figure 6 - supplement 1. Increased left-right variability of posterior lobe phenotype upon**
1003 ***dumpy* knockdown.**

1004 (A) Comparison of *dumpy* knockdown (purple circles) and control knockdown (green squares) of
1005 left and right adult posterior lobes in single individuals grown at 29°C measuring height at the
1006 ventral side of the posterior lobe (represented as a single dot or square). Black line represents
1007 perfect correlation in height. *dumpy* knockdown individuals stray more from perfect correlation,
1008 indicating that the height of the posterior lobe varies more in the *dumpy* knockdown. (B)
1009 Percentage of *dumpy* knockdown individuals plotted in (A) in which both posterior lobes were
1010 classified as the same phenotype or different phenotypes (defined in Figure 6).

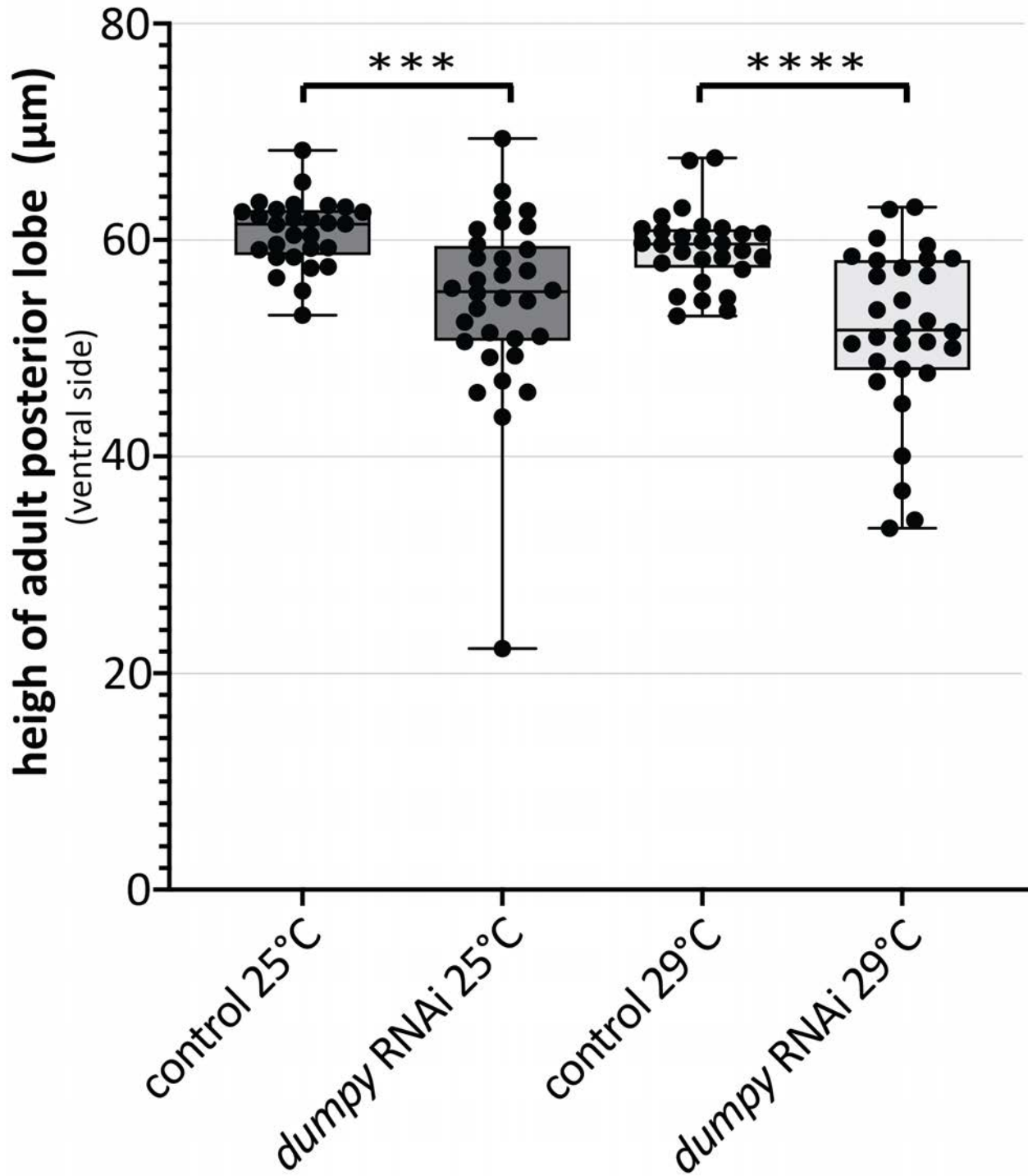
1011 Figure 7



1012 **Figure 7. Correlation between the deposition of Dumpy and knockdown phenotype.**

1013 (A-B) Comparison of *mCherry* RNAi (control) and *dumpy* RNAi at 44 hours APF (A) and 52
1014 hours APF (B). Images are rotated in 3D to visualize the full shape of the posterior lobe labeled
1015 with E-cadherin. Quantification of tissue height at the ventral tip (dark blue) and dorsal base
1016 (light blue) of the lobe. Cartoon represents relative location of cross-section used for tissue
1017 thickness measurement. Individual data points presented; n=at least 10 per each time point.
1018 The ventral tip is defined as the location where the posterior lobe is max thickness. The base
1019 was determined by moving 19.76 μ m dorsally from the ventral tip. Statistical significance for
1020 each time point indicated (unpaired t-test; *** $p \leq 0.001$; n.s.=not significant $p \geq 0.05$). (C-F)
1021 Comparison of *mCherry* RNAi (control) (C & E) and *dumpy* RNAi (D & F) at 44 hours APF and
1022 52 hours APF with Dumpy:YFP (Green) and Ecad (Magenta). GFP antibody was used to
1023 increase YFP signal. All cross-sections are oriented with apical side at the top and basal side at
1024 the bottom. Relevant structures labeled: Lateral plate (LP) posterior lobe (PL), and clasper (C).
1025 Cross-sections are max projections of 5.434 μ m sections to show full Dumpy connection. Images
1026 were independently brightened to show relevant structures. Scale bar, 20 μ m. n=at least 5 per
1027 experiment.

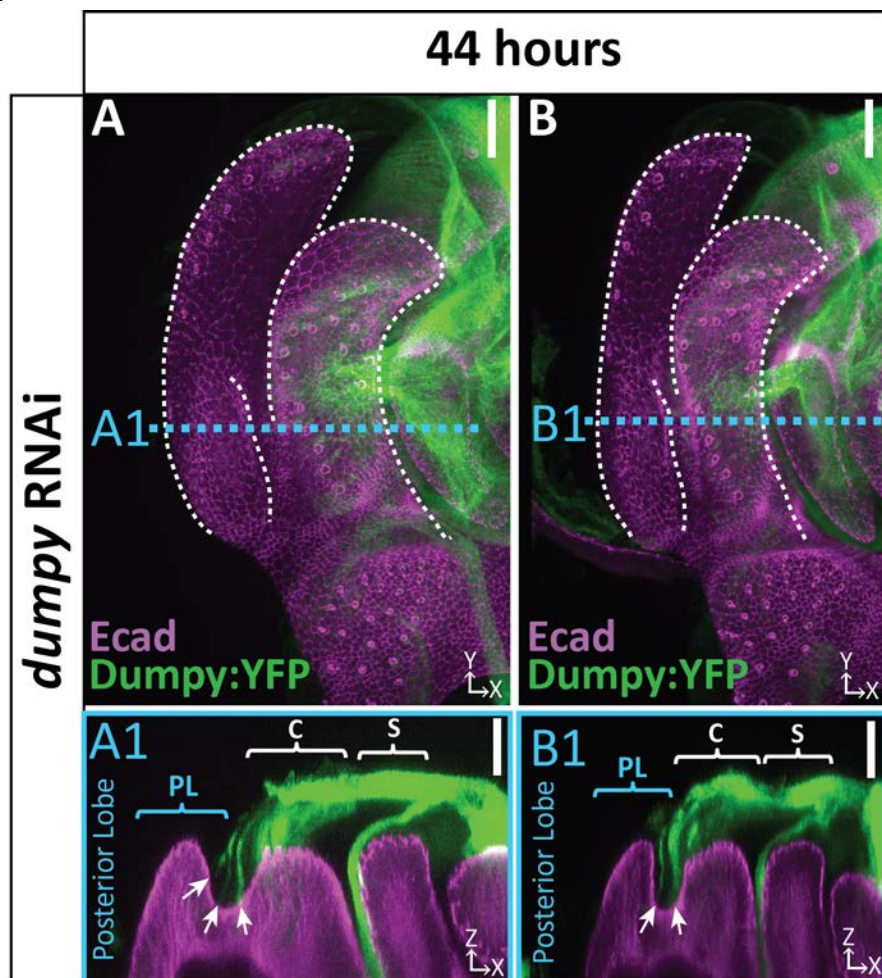
1028 Figure 7 – supplement 1



1029 **Figure 7 - supplement 1. Variability in height of posterior lobe in *dumpy* knockdown.**
1030 Comparison of *mCherry* RNAi (control) and *dumpy* RNAi adults. Quantification of height of
1031 cuticle at the ventral side of the posterior lobe. (unpaired t-test; *** $p \leq 0.001$; **** $p \leq 0.0001$; $n \geq 28$).
1032

1033 **Figure 7 – supplement 2**

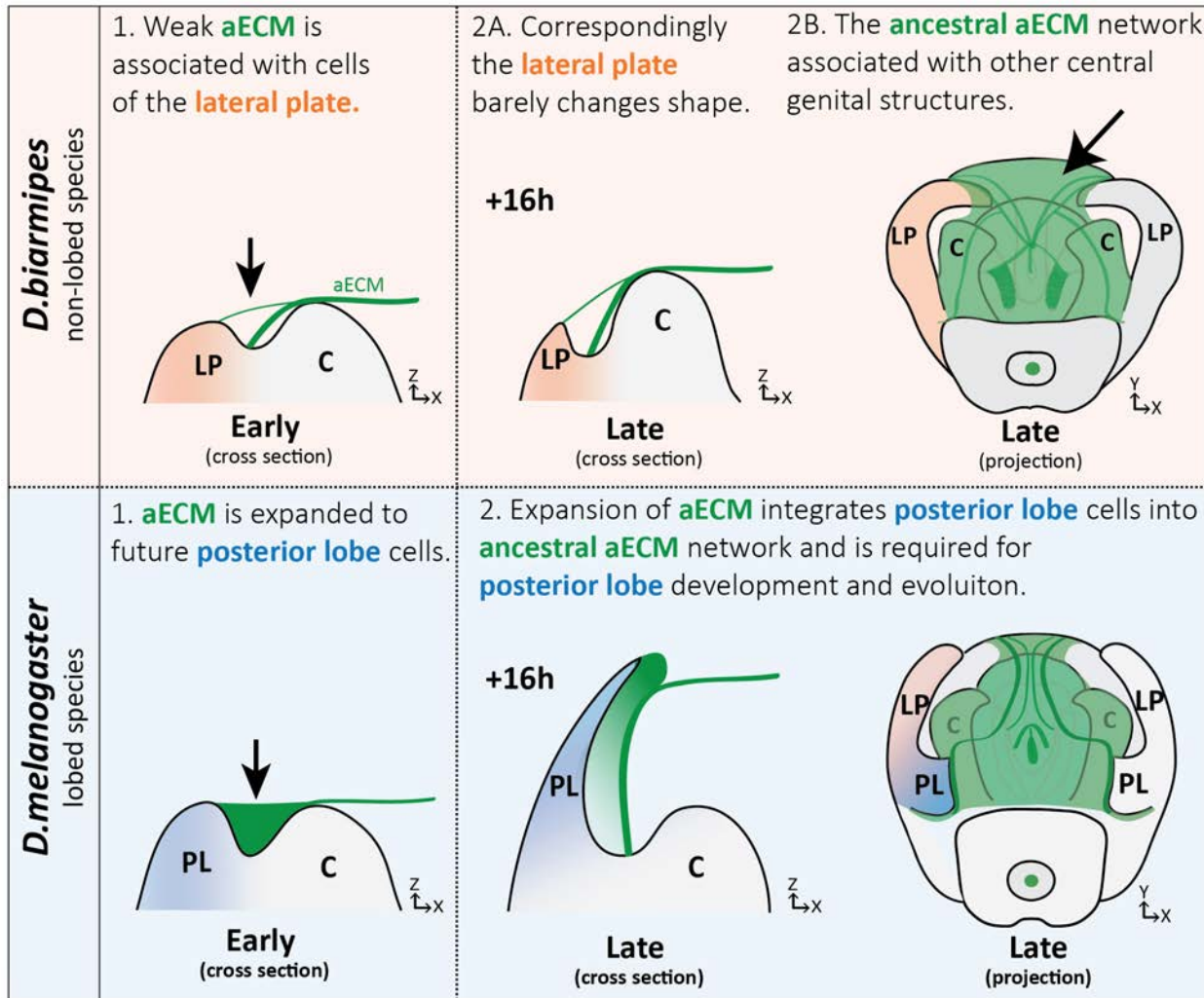
1034



1035 **Figure 7 - supplement 2. Strands of Dumpy in *dumpy* knockdown.**

1036 (A & B) *dumpy* RNAi at 44 hours APF with Dumpy:YFP showing strands of Dumpy connecting to the
1037 crevice between the lateral plate and clasper (arrow). Relevant structures labeled: Lateral plate (LP)
1038 posterior lobe (PL), and clasper (C). Cross-sections are max projection of 5.434µm section to show full
1039 Dumpy connection. Scale bar, 20µm.

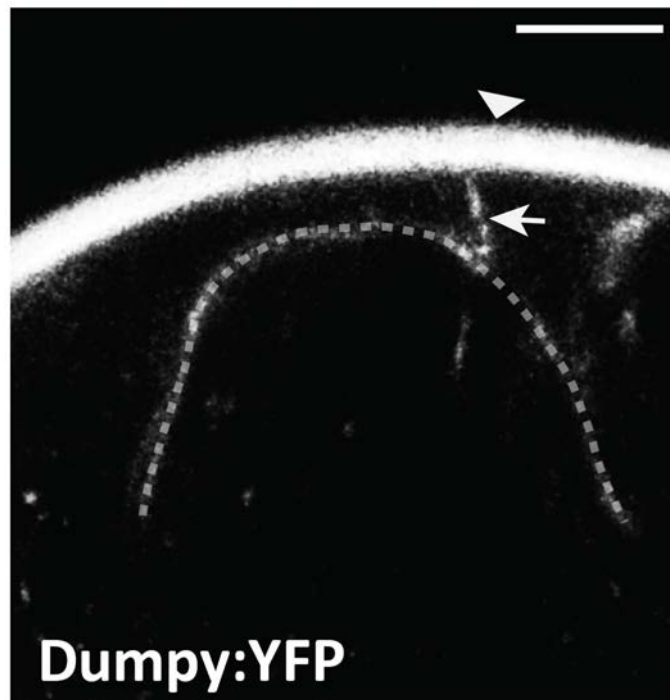
1040 **Figure 8**



1041 **Figure 8. Expansion of aECM associated with the evolution of a novelty.**

1042 (Top) Illustration of non-lobed species, *D. biarmipes*, with ancestral aECM network covering
1043 central genital structures (2B) including the clasper (C), sheath, and phallus. Weak connections
1044 of aECM span from the clasper to the lateral plate (LP) during early development (1 & 2A - top).
1045 (Bottom) Illustration of lobed species, *D. melanogaster*. The aECM network has expanded to fill
1046 the crevice between the lateral plate and clasper (1-bottom) integrating these cells into the
1047 ancestral aECM network (2-bottom). This aECM population is needed for cells to properly
1048 project from the lateral plate, forming the posterior lobe.

1049 **Figure 8 – supplement 1**



1050 **Figure 8 - supplement 1. Dumpy anchors posterior spiracles to surrounding cuticle.**

1051 Live imaging of Dumpy:YFP in the embryonic posterior spiracles. Posterior spiracle (dotted line)

1052 is connected to the cuticle (arrowhead) via a tether of dumpy (arrow). Scale bar, 20 μ m.